I. Seasonal Changes in Titan's Cloud Activity
II. Volatile Ices on Outer Solar System Objects

Thesis by

Emily L. Schaller

In Partial Fulfillment of the Requirements

for the Degree of

Doctor of Philosophy

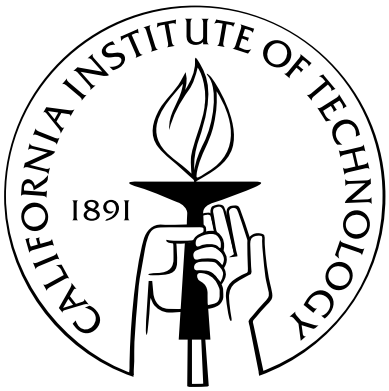

California Institute of Technology

Pasadena, California

2008

(Defended April 28, 2008)

Acknowledgements

I would first like to thank my parents Meg and Dave Schaller. Starting with the picture book of the solar system when I was five years old and continuing throughout my PhD they have always been supportive of my love of science. This thesis is dedicated to them.

I next want to thank Dave Lamb for his love and support throughout this process. I've actually really enjoyed being a grad student and I think that has been in large part due to the people in GPS. I thank my advisor Mike Brown, for his support and willingness to let me dive in and explore different areas of planetary science that were interesting to me — even if they weren't exactly what I was supposed to be doing. I really value all that I have learned from him and the tools he has given me over these past few years. Thanks to all the people who have passed through Mike's group including Antonin Bouchez, Chad Trujillo, Henry Roe, Lindsey Malcolm, Sarah Horst, Kris Barkume, Darin Ragozzine, and Meg Schwamb: I have learned something from each of them. Thanks to Kris Barkume for her friendship and for those late night bottles of wine. I thank my roommates (Rowena Lohman, Colette Salyk, Amy Hofmann, and, of course, Harry the cat) for putting up with me. Thanks also to the squash/salsa crew including Margarita Marinova, Oded Aharonson, Jenny Meyer, and Jack Wisdom. Thanks to Henry Roe for getting me started with Titan observing and IDL programming and Mate Adamkovics for providing me with his Titan radiative transfer code.

Finally, I especially want to thank all of the support astronomers and telescope operators at Keck, Palomar, IRTF, and NM Skies with whom I've worked over these

past few years (there are many but a few stick out in my mind the most) — Joel Aycock, Randy Campbell, Bill Golish, Dave Griep, Mark Kassis, Jim Lyke, Mike Rice, Paul Sears, and Cindy Wilburn. Their hard work and attention to detail was what made all the observations in this thesis possible.

Abstract

This thesis presents studies in two distinct areas of observational planetary astronomy: studies of Saturn's moon Titan's seasonally varying tropospheric clouds, and studies of the surface compositions of Kuiper belt objects.

I. Understanding Titan's methane-based hydrological cycle and interpreting how and when the fluvial surface features seen by the Cassini Spacecraft were formed requires frequent long-term observations of Titan's clouds. Using nearly 100 adaptive optics images from the Keck and Gemini Telescopes from 2002–2006, we mapped the locations, frequencies, and magnitudes of Titan's clouds. We also developed a near-nightly cloud-monitoring program with the NASA Infrared Telescope Facility (IRTF). Nightly whole-disk infrared spectroscopy with IRTF allows us to determine Titan's total fractional cloud coverage, magnitudes, and altitudes, complementing and providing context for the relatively infrequent Cassini flybys. Taken together, the observations presented in this thesis have shown a striking seasonal change in the behavior of Titan's clouds as Titan has moved from southern summer solstice (October 2002) toward vernal equinox (August 2009) and indicate that seasonally varying insolation appears, to first order, to control Titan's cloud locations (Schaller et al. 2006a & 2006b).

II. Unlike Pluto and Eris, the vast majority of Kuiper belt objects (KBOs) are too small and too hot to retain volatile ices like CH_4, N_2, and CO on their surfaces to the present day. As a result, their infrared spectra are either dominated by involatile water ice or dark spectrally featureless material. To understand the dichotomy between volatile-rich and volatile-free surfaces in the outer solar system, we constructed a

model of atmospheric escape of volatile ices over the age of the solar system (Schaller & Brown 2007a). We predicted that Quaoar, an object about half the size of Pluto, should be just capable of retaining methane ice to the present day. We observed Quaoar with the Keck Telescope, used Hapke theory to model its spectrum, and found that it contains a small amount of methane on its surface, indicating that it is a transition object between the dominant volatile-poor small KBOs and the few volatile-rich KBOs such as Pluto and Eris (Schaller & Brown 2007b).

Contents

Acknowledgements **iii**

Abstract **v**

1 Introduction **1**

1.1 Seasonal Changes in Titan's Cloud Activity 3

1.1.1 A Large Cloud Outburst at Titan's South Pole 3

1.1.2 Dissipation of Titan's South Polar Clouds 4

1.1.3 Seasonal Change on Titan Observed with IRTF/SpeX 4

1.2 Volatile Ices on Outer Solar System Objects 5

1.2.1 Volatile Loss and Retention on Kuiper Belt Objects 6

1.2.2 Detection of Methane on (50000) Quaoar 7

2 A Large Cloud Outburst at Titan's South Pole **11**

2.1 Abstract 13

2.2 Introduction 13

2.3 Observations 15

2.4 Results 18

2.5 Discussion 21

3 Dissipation of Titan's South Polar Clouds **29**

3.1 Abstract 31

3.2 Introduction 31

3.3 Observations and Results 36
3.4 Discussion 40

4 Seasonal Change on Titan Observed with IRTF/SpeX 51
4.1 Abstract 53
4.2 Introduction 53
4.3 Observations 56
4.4 Results 57
4.4.1 Lightcurves 57
4.4.2 Clouds 62
4.4.3 Search for CO_2 Ice 63
4.5 Discussion 67
4.6 Conclusions 69

5 Volatile Loss and Retention on Kuiper Belt Objects 79
5.1 Abstract 81
5.2 Introduction 81
5.3 Atmospheric Escape 82
5.4 Results and Discussion 85

6 Detection of Methane on Kuiper Belt Object (50000) Quaoar 95
6.1 Abstract 97
6.2 Introduction 97
6.3 Observations 98
6.4 Spectral Modeling 99
6.5 Discussion 103

List of Figures

2.1 Keck adaptive optics images of cloud outburst 16
2.2 Flux comparison with 1995 cloud event 20

3.1 Mean daily insolation at the top of Titan's atmosphere 37
3.2 Titan cloud locations with time 39
3.3 Keck and Gemini Titan adaptive optics images 41

4.1 Titan near-infrared spectrum 56
4.2 H & K Band Titan spectra 58
4.3 K-band lightcurves 60
4.4 Titan lightcurve magnitude with wavelength 61
4.5 Residual Titan spectra 64
4.6 Fractional cloud coverage of Titan's disk 65
4.7 Titan's 2.11–2.12 micron lightcurve with RT model 66
4.8 Non-detection of CO_2 ice 67

5.1 Volatile loss as a function of KBO temperature and radius 87

6.1 Quaoar spectrum with best-fit models 101
6.2 Quaoar ratio spectrum with best-fit models 102

Chapter 1

Introduction

http://www.ifa.hawaii.edu/images/aerial-tour/northeast.html

1.1 Seasonal Changes in Titan's Cloud Activity

Discovered in 1655 by Christiaan Huygens, Titan still remains one of the most mysterious objects in the solar system. The temperature and pressure conditions at the surface near the triple point of methane mean that Titan is capable of possessing an alien meteorological cycle analogous to Earth's hydrological cycle but with methane as the condensable species. Titan's small angular size as seen from Earth (∼0.8") prevented directly resolving it until the Voyager encounter in 1980. Though Voyager was able to observe Titan's entire disk, its cameras could not penetrate Titan's thick stratospheric haze that obscured the surface and lower atmosphere from view. Investigators in the 1990's realized that there were narrow window regions in the near infrared through which photons could penetrate to Titan's surface (Lemmon et al., 1993; Griffith, 1993). Spectroscopy across these windows revealed Titan's strong lightcurve due to albedo variations on its surface and variable tropospheric clouds that were inferred to cover between 0–8% of Titan's disk (Griffith et al., 1998, 2000).

In Chapters 2, 3, and 4 of this thesis, we present ground-based observations of Titan using a variety of different telescopes and techniques to observe Titan's variable tropospheric clouds. Though the data presented in this thesis comprise only 6 earth years (equivalent to less than one season on Titan) we were fortunate to have observed Titan during two very different eras of cloud activity. We compare these observations with predictions of how Titan's cloud activity should evolve over the course of its ∼29.7 year seasonal cycle.

1.1.1 A Large Cloud Outburst at Titan's South Pole

Chapter 2 (Schaller et al., 2006a) discusses a brightening of Titan's clouds observed with the Keck adaptive optics system immediately before the arrival of the Cassini spacecraft into orbit around Saturn (October 2004). This brightening was the largest ever seen in Titan adaptive optics images. We show that this brightening was con-

sistent in magnitude with a similar event observed in September 1995 by Griffith et al. (1998) who saw Titan's cloud activity increase by nearly a factor of 10 relative to all previous observations over two nights. The fact that two of these large cloud events have been caught by ground-based observers (one 2 years post southern summer solstice and one near autumnal equinox) indicates that these events may be fairly common on Titan.

We discuss several scenarios that may explain why Titan has such violent cloud outbursts and note the role these events might play in shaping the geologic features observed on the surface of Titan.

1.1.2 Dissipation of Titan's South Polar Clouds

Chapter 3 (Schaller et al., 2006b) discusses the disappearance of Titan's south polar clouds observed in Keck and Gemini adaptive optics images beginning two years after the end of Titan southern summer solstice. Beginning in December 2004 (only two months following the large cloud outburst discussed in Chapter 2), Titan's south polar cloud activity decreased to undetectable levels. In nearly all images and spectra taken prior to December 2004 at least a small amount of cloud activity was observed near the south pole. However, between December 2004 and the present, cloud activity near Titan's south pole has essentially stopped. We discuss the timing of this south polar cloud cessation and discuss how it is roughly consistent with Titan's south pole ceasing to be the area of maximum solar insolation. We also note that the breakup of the south polar cloud system might have also been related to surface cooling or condensation nuclei clearing out as a result of the large cloud event observed only months earlier.

1.1.3 Seasonal Change on Titan Observed with IRTF/SpeX

Chapter 4 presents observations from an ongoing near-nightly monitoring program begun in February 2006 with the NASA Infrared Telescope Facility (IRTF). This

program was initially motivated by photometric observations we carried out with a robotic 14" telescope in New Mexico. We performed whole disk photometry of Titan through two filters which probed to different levels in Titan's atmosphere in the visible region of the spectrum. The ratio of the total flux of Titan in a methane window (750 nm), to the flux in a methane absorption region (795 nm) allowed us to detect Titan's surface lightcurve and large increases in cloud activity, such as the event discussed in Chapter 2. Though the 14" telescope could detect large events, the small-scale daily clouds were undetectable. In addition, in order to achieve the required signal-to-noise to detect the surface lightcurve, Titan needed to be observed for at least 4 hours each night.

The 3.0 m NASA Infrared Telescope facility equipped with its spectrometer (SpeX) allows us to obtain a complete spectrum from 0.8–2.4 μm in only three minutes of integration time. These spectra cover six Titan window regions where photons penetrate to Titan's surface and lower atmosphere. This program duplicates on a larger scale observations done in the 1990s with the United Kingdom Infrared Telescope (UKIRT) and allows direct comparisons with that dataset, taken near autumnal equinox. The flexible scheduling of the IRTF allows near-nightly observations and provides the type of dataset that Cassini, with its relatively infrequent Titan flybys, is incapable of providing. In the two years of IRTF observations, we have observed a striking seasonal difference in the behavior of Titan's clouds between the present season and similar observations from 1993–1999. We discuss the implications of these observations and compare them with the predictions of Titan General Circulation Models.

1.2 Volatile Ices on Outer Solar System Objects

There are now over 1100 known objects orbiting the the sun with perihelia beyond Neptune's orbit. The existence of this belt of debris left over from planetary accretion was first proposed by Kuiper (1951) but only recently detected. While the orbits of

Kuiper belt objects (KBOs) have provided many insights about the early dynamical history of the solar system (see Malhotra et al. (2000) and references therein), detailed physical and chemical studies of individual objects are now beginning to yield valuable information about the formation and evolution of these bodies themselves.

The advent of large (6+ meter) telescopes with sensitive near-infrared spectrographs, along with the new discoveries of KBOs that rivaled or even exceeded the size of Pluto, lead to an expansion of research on the surface compositions of these bodies. Near infrared spectroscopy is particularly well suited for studying the surfaces of outer solar system bodies as many molecules expected to be present on these objects (such as water ice, methane, nitrogen, ammonia, and higher-order hydrocarbons) have absorption bands in the 1.4–2.5 micron region.

The near-infrared spectra of the known KBOs divide into three general categories: methane-rich, water-ice rich, and featureless. The largest objects, including Pluto, Eris, Sedna, 2005 FY9, and Neptune's moon Triton (thought to be a captured KBO), are dominated by absorptions due to methane ice (Owen et al., 1993; Cruikshank et al., 1993; Brown et al., 2005; Barucci et al., 2005; Brown et al., 2007). A second class of objects, that are generally smaller than the methane-rich objects, contain varying amounts of water-ice on their surfaces (Barkume et al., 2008). The final class have featureless spectra in the infrared with nothing identifiable (Barkume et al., 2008).

In Chapters 5 and 6 of this thesis we focus on understanding why the methane-rich KBOs are capable of retaining methane (and other supervolatiles like carbon monoxide and molecular nitrogen) on their surfaces to the present day and why most KBOs are not.

1.2.1 Volatile Loss and Retention on Kuiper Belt Objects

In Chapter 5 (Schaller & Brown 2007a) we calculate rates of volatile loss on outer solar system bodies. The wide variety of Kuiper belt objects with different sizes and

at different heliocentric distances provides us with a kind of laboratory in which to test predictions of volatile loss and retention. Assuming the slowest possible escape rates and integrating this escape flux over an object's orbit, we were able to determine the minimum amount of loss of methane, carbon monoxide and molecular nitrogen that must have occurred on all the known KBOs and centaurs over the age of the solar system. If this minimum loss was greater than the initial amount of volatiles estimated to be present on the body, then there should be no volatile ices present on the surface of that object.

We applied our model to all the known KBOs and centaurs and found that in addition to Pluto, Triton, Sedna, and Eris, there were three objects that were near the transition region between certain volatile loss and possible volatile retention: 2005 FY9, 2003 EL61, and Quaoar. The presence of 2005 FY9 near this transition region provided an explanation for the depletion of nitrogen seen by Brown et al. (2007). 2005 FY9 is capable of possessing methane ice but not capable of possessing molecular nitrogen due to its size and the effective temperature it experienced over the past 4.5 billion years. 2003 EL61 is known to have a water-ice dominated spectrum and is the parent body of the first collisonal family known in the Kuiper Belt (Brown et al., 2007b). The fact that this object does not have any volatile ices on its surface is not surprising because the massive collision it experienced stripped off most of its icy mantle and likely any volatiles it possessed as well. The final potentially volatile-rich object, Quaoar, a body about half the size of Pluto with a perihelion about 10AU further from the sun, had been observed by Jewitt & Luu (2004) who found crystalline water-ice and ammonia ice on the surface. Due to this object's potential to contain volatile ices, we determined that additional observations were warranted.

1.2.2 Detection of Methane on (50000) Quaoar

In Chapter 6 (Schaller & Brown 2007b), we present medium-resolution (R$\sim$2000) near-infrared spectral observations of Quaoar taken over three nights with NIRSPEC

on the Keck II telescope in April 2007. The goal of these observations was to determine if any volatile ices were present on the surface. We modeled the spectrum using Hapke theory and found that with a 6 times higher signal-to-noise per pixel than Jewitt & Luu (2004), the feature at 2.2 μm previously identified as ammonia hydrate is in fact due to methane ice.

We predicted in Chapter 5 that Quaoar should be barely capable of retaining methane ice on its surface to the present day. The detection of a small amount of methane on Quaoar indicates that the last stages of volatile loss on an object may occur quite slowly. As more objects are discovered with high perihelia similar to Sedna, we expect that even the smallest of these objects may be capable of containing volatile ices like methane, molecular nitrogen, and carbon monoxide on their surfaces.

Bibliography

Barkume, K. M., Brown, M. E., & Schaller, E. L. 2008, Astronomical Journal, 135, 55

Barucci, M. A., Cruikshank, D. P., Dotto, E., Merlin, F., Poulet, F., Dalle Ore, C., Fornasier, S., & de Bergh, C. 2005, Astronomy and Astrophysics, 439, L1

Brown, M. E., Barkume, K. M., Blake, G. A., Schaller, E. L., Rabinowitz, D. L., Roe, H. G., & Trujillo, C. A. 2007a, Astronomical Journal, 133, 284

Brown, M. E., Barkume, K. M., Ragozzine, D., & Schaller, E. L. 2007b, Nature, 446, 294

Brown, M. E., Trujillo, C. A., & Rabinowitz, D. L. 2005, Astrophysical Journal, Letters, 635, L97

Cruikshank, D. P., Roush, T. L., Owen, T. C., Geballe, T. R., de Bergh, C., Schmitt, B., Brown, R. H., & Bartholomew, M. J. 1993, Science, 261, 742

Griffith, C. A. 1993, Nature, 364, 511

Griffith, C. A., Hall, J. L., & Geballe, T. R. 2000, Science, 290, 509

Griffith, C. A., Owen, T., Miller, G. A., & Geballe, T. 1998, Nature, 395, 575

Jewitt, D. C. & Luu, J. 2004, Nature, 432, 731

Kuiper, G. P. 1951, Proceedings of the National Academy of Science, 37, 1

Lemmon, M. T., Karkoschka, E., & Tomasko, M. 1993, Icarus, 103, 329

Malhotra, R., Duncan, M. J., & Levison, H. F. 2000, Protostars and Planets IV, 1231

Owen, T. C., Roush, T. L., Cruikshank, D. P., Elliot, J. L., Young, L. A., de Bergh, C., Schmitt, B., Geballe, T. R., Brown, R. H., & Bartholomew, M. J. 1993, Science, 261, 745

Schaller, E. L. & Brown, M. E. 2007a, Astrophysical Journal, Letters, 659, L61

Schaller, E. L. & Brown, M. E. 2007b, Astrophysical Journal, Letters, 670, L49

Schaller, E. L., Brown, M. E., Roe, H. G., & Bouchez, A. H. 2006a, Icarus, 182, 224

Schaller, E. L., Brown, M. E., Roe, H. G., Bouchez, A. H., & Trujillo, C. A. 2006b, Icarus, 184, 517

Chapter 2

A Large Cloud Outburst at Titan's South Pole

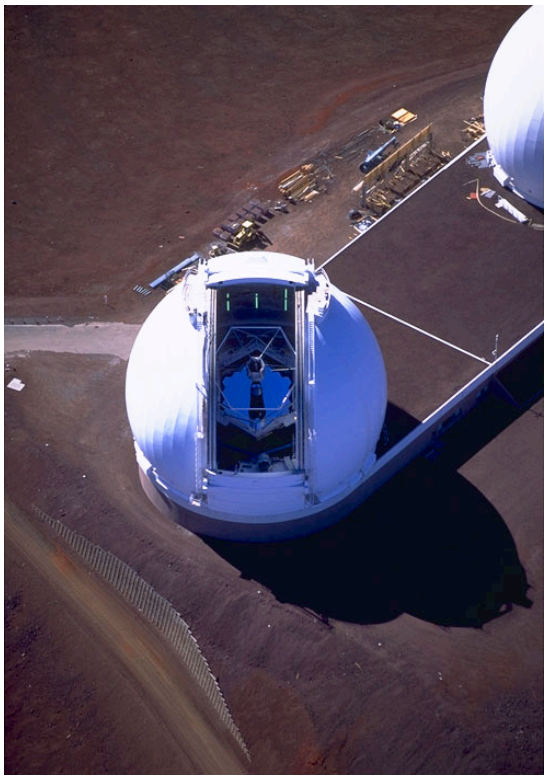

http://www.ifa.hawaii.edu/images/aerial-tour/keck2-60b.jpg

This chapter has been published in its entirety under the same title by authors E.L. Schaller, M.E. Brown, H.G. Roe, and A.H. Bouchez in *Icarus*, 2006, Volume 182, pp. 224–229.

2.1 Abstract

Images of Titan acquired over five nights in October 2004 using the adaptive optics system at the Keck Observatory show dramatic increases in tropospheric cloud activity at the south pole compared with all other images of Titan clouds to date. During this time, Titan's south polar clouds brightened to more than 18 times their typical values. The Cassini Ta flyby of Titan occurred as this storm was rapidly dissipating. We find that the brightness of this cloud outburst is consistent with the dramatic transient brightening of Titan observed in atmospheric windows on two nights in 1995 by Griffith et al. (1998) if we scale the brightness of the cloud by projecting it onto the equator. While apparently infrequent, the fact that large cloud events have been observed in different seasons of Titan's year indicates that these large storms might be a year-round phenomenon on Titan. We propose possible mechanisms to explain these occasional short-term increases in Titan's cloud activity.

2.2 Introduction

Data from the Voyager encounter with Saturn's moon Titan first suggested that Titan might support a methane meteorological cycle including convective methane clouds and rain beneath the smoggy stratospheric haze (Eshleman et al. 1983; Flasar 1983; Lunine et al. 1983; Toon et al. 1988). Observations with ground-based telescopes in narrow methane windows in the infrared found that Titan's surface was not of uniform albedo but instead had a reproducible infrared lightcurve with maximum brightness occurring near 110 W longitude (Coustenis et al. 1995; Griffith 1993; Lemmon et al. 1995). HST images (Meier et al. 2000; Smith et al. 1996) and early adaptive optics images (Combes et al. 1997) revealed a continent sized bright feature centered near 110 W longitude now known as Xanadu. None of these observations detected any evidence for transient clouds in Titan's atmosphere.

Transient cloud activity in Titan's troposphere was first detected spectroscopically

by Griffith et al. (1998) who reported a dramatic brightening of Titan in atmospheric windows during two nights in September of 1995 compared with observations on twelve other nights from 1993-1997. They found that this brightening corresponded to ∼9% cloud cover of Titan's disk and placed the clouds at an altitude of 15 km. Griffith et al. (2000) then reported evidence for smaller scale transient cloud activity occurring on several nights in 1993-1999. These daily clouds were much smaller than the large cloud event witnessed in 1995 and covered less than 1% of Titan's disk.

The first images of Titan's clouds were obtained by Brown et al. (2002) and Roe et al. (2002) using the adaptive optics systems on the Keck and Gemini telescopes. Since then, clouds have regularly been observed near Titan's south pole (Bouchez & Brown, 2005; Gendron et al., 2004; Roe et al., 2005a) and typically contribute about 1% of the total brightness of Titan's disk, consistent with the daily clouds observed spectroscopically by Griffith et al. (2000). The location of the clouds near the south pole lead Brown et al. (2002) to suggest that they may form via insolation driven convection because the south pole was the area of maximum solar insolation on Titan (southern summer solstice was in October 2002). The presence of south polar tropospheric clouds at this season is likely controlled in a complex way by both the insolation and the global circulation leading to uplift at the pole. South polar clouds may also form non-convectively by cooling of air parcels as they move poleward (Barth & Toon, 2004).

Between 2001 and mid-2004 clouds had been observed near the south pole of Titan on 66 occasions in Palomar, Keck and Gemini images (Bouchez & Brown, 2005; Bouchez et al., 2004), but at most times the clouds covered no more than 1% of the surface, and at no time did the coverage approach that seen by Griffith et al. (1998). The lack of large cloud features suggested a possible difference in the cloud formation mechanisms between the current south polar summer season and the spring equinox season when the large cloud was observed in 1995.

We report here on a dramatic brightening of Titan's south polar clouds observed

on five nights in October 2004 with Keck adaptive optics images and compare the brightness of this cloud outburst to the transient brightening observed in 1995 by Griffith et al. (1998).

2.3 Observations

Images of Titan presented here were taken with the W.M. Keck 10-m telescope using the adaptive optics system and the NIRC2 near-infrared camera (Wizinowich et al., 2000) through three different filters that probe to different levels in Titan's atmosphere. Images taken through the K' filter (2.03-2.36 um) probe to Titan's surface, while those taken through the H22 (1-0) filter (2.11-2.14 um) probe to ∼10 km altitude (lower troposphere), and the Bγ filter (2.15-2.18 um) probes to ∼50 km altitude (lower stratosphere). In Titan's atmosphere, photons of the wavelength range seen through the H2 filter reach an optical depth of unity in the lower troposphere owing to absorption by methane, nitrogen, and hydrogen (Roe et al., 2002). Images in the H2 filter therefore show only light scattered in Titan's atmosphere above an altitude of about 10 km, thus this filter is ideal for detecting clouds in the middle of Titan's troposphere without the confusion of surface features. We therefore use the H2 filter for our analysis of cloud locations and magnitudes. Images were flat-fielded, corrected for bad pixels, and oriented so that Titan's north pole is aligned with the vertical axis. At the time of the observations Titan was at a distance of 9.2 AU, so the Keck telescope diffraction limited resolution of 0.05 arcseconds corresponds to 330 km on the surface of Titan.

Figure 1a shows images of Titan from seven nights in 2003 that are typical of the cloud activity seen during this season. Beginning with images on 28 September 2004, however, Titan's south polar cloud system brightened dramatically. This brightening was observed over the course of six nights from 28 September until 28 October (Fig. 1b), when the brightness of Titan's south polar clouds returned to their typical values.

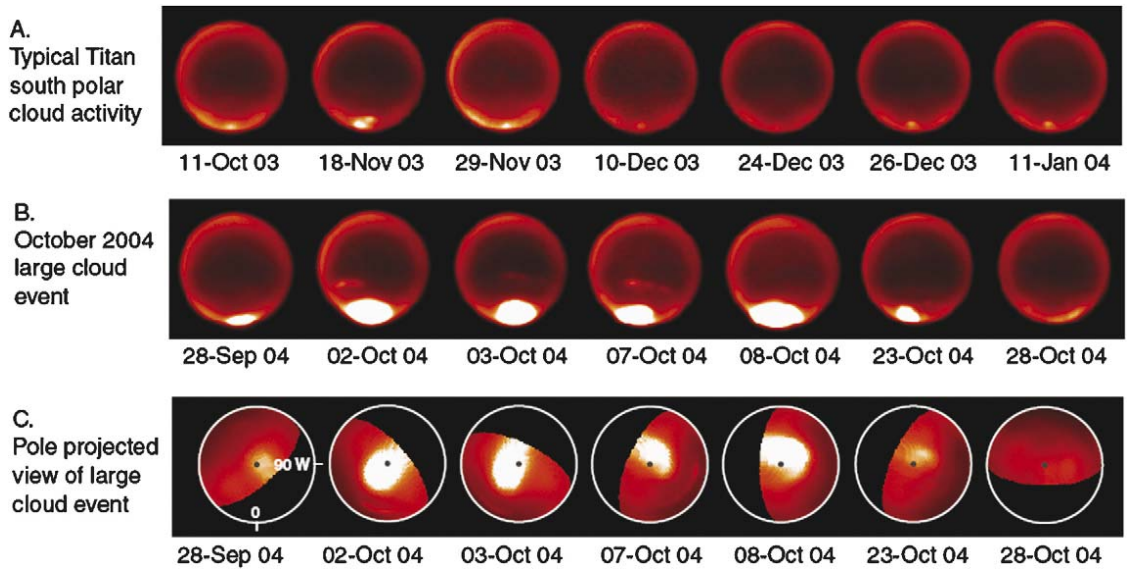

Figure 2.1 a. Keck adaptive optics images of Titan taken through the H2(1-0) (2.11-2.14) filter oriented with Titan north up. This filter probes only to Titan's troposphere making it ideal for observing Titan's clouds. A. Images of Titan from seven nights in 2003 that are typical of the low levels of cloud activity seen from 2001-2004. B. Cloud activity at the south pole is seen in all seven of these images and dramatic brightening is observed in images from October 2, 3, 7, 8, 2004. C. Pole projected images of Titan's clouds with the pole location marked with a black dot. All images have Titan 0W longitude pointing up. The Cassini 004, by which point cloud activity was rapidly dissipating. By October 28, 2004 cloud activity had dissipated down to typical levels of less than 1% cloud coverage (Bouchez & Brown, 2005). These images also allow us to constrain the duration of the cloud outburst to less than 30 earth days. Locations of the clouds also indicate that convection on Titan is extremely vigorous and that large clouds can dissipate and reform in several days.

At the peak of the cloud outburst on 8 October, the cloud covered at least 8% of the disk of Titan. Also visible in the images from October 2, 3, and 7 are smaller clouds located at mid-latitudes. These clouds are discussed in detail by Roe et al. (2005b) and will not be discussed here.

Titan's clouds are typically not detected or are very faint in Bγ images indicating that they are located in the troposphere at an altitude below that which photons of the wavelength range of the Bγ filter can penetrate ($\sim$50 km) ((Roe et al., 2002). In addition, all other measurements of Titan cloud altitudes (Griffith et al., 1998, 2000; Brown et al., 2002; Griffith et al., 2005) placed these clouds in the troposphere. Though the large south polar cloud can be seen in several of the Bγ images, the contribution of the cloud to the total brightness of Titan in the H2(1-0) filter is over five times greater than that in the Bγ filter. A typical cloud with a brightness of 1% in the H2 (1-0) filter would not be detected in the Bγ filter were it over five times fainter, consistent with our observations. Therefore, given that all previous measurements of Titan cloud heights place them in the troposphere and the brightness of the large clouds in the Bγ filter is below that which could be detected were these clouds of typical size, we assume that these clouds are also located in the troposphere.

To find the extent of Titan's brightening due to the presence of these clouds, we first photometrically normalized each image by measuring the total brightness of Titan in the H2 filter and scaling the brightness of the image by the total flux of the relatively unchanging northern half of Titan. We then subtracted the total flux from images of Titan with clouds from the total flux from images of Titan without clouds (28 October 2004, 10 January 2004, 24 December 2003, 25 December 2003). These images with no distinct clouds show only photons scattered from the slowly-changing haze in the stratosphere of Titan. Because of possible long term changes in the haze abundance, we attempt to use closely spaced dates for comparison when possible. However we found only about a 1% difference in cloud brightness regardless of the comparison date used, and we use this value as our estimate of the error in

our measurement. The fractional increase in Titan's total flux through the H2 filter compared with Titan's total flux on nights with low cloud activity is presented in Figure 2. We find that the total flux of Titan through the H2 filter increased by 18% on the brightest observed night of the outburst (October 8, 2004).

2.4 Results

The cloud outburst of October 2004 was significantly larger than any other directly imaged on Titan. To compare the magnitude of this outburst to the Griffith et al. (1998) cloud event detected spectroscopically in 1995, we measure the magnitude of brightening in the H2 filter wavelength region (2.11-2.14 um) of the Griffith et al. (1998) spectra from September 4 and 5 1995. We find that the total flux of Titan increased by 36% and 59% in the H2 filter wavelength region for September 4 and 5 respectively (Fig 2). Thus the large cloud event of October 2004, though it is the largest south polar cloud seen in several years of monitoring Titan (Schaller et al., 2005), is still 3.3 times fainter than the brightest transient brightening attributed to clouds in 1995.

Griffith et al. (1998), however, suggest that, based on spectral changes from 4 to 5 September, the cloud they observed is consistent with an equatorial location. Such a location would be consistent with the hypothesis that convective clouds form near the latitude of maximum solar insolation (Brown et al., 2002), which was near the equator at the southern spring equinox season of the 1995 observations. The brightness of the 2004 outburst is significantly attenuated relative to a comparably large cloud system near the center of Titan's disk both from geometric foreshortening and from additional methane, nitrogen, and hydrogen opacity through a longer atmospheric path length. If we move the October 2004 clouds from their locations near the pole (see Table 1) to the center of Titan's disk, we find that they would appear brighter by a factor of 1.7 due to geometric foreshortening. In addition, by following the method

of Roe et al. (2002) we find that the decreased gas opacity through a shorter path length would increase the observed brightness of the clouds by an additional factor of 2. Combining these two effects, we find that the 2004 clouds would have appeared brighter by at least a factor of ∼3.5 if they were near the equator. Therefore if the 2004 cloud event were at the equator, it would have appeared to be of comparable brightness to the 1995 event (Fig. 2 dashed line).

These observations also allow us to constrain the duration and short-term variability of large cloud events. From the seven Keck images we can constrain the duration of the cloud outburst to less than 30 earth days. In addition, observations on sequential nights indicate that the flux from the storm can stay relatively constant (October 2 & 3) or increase by a factor of two (October 7 & 8) in only 24 hours. Rapid variability in cloud flux was also observed by Griffith et al. (1998) during the two nights of the 1995 storm. This variation may have been due to parts of the cloud rotating onto the limb but may have also been due to rapid fluctuation in cloud size or height.

The locations of brightest pixels of the clouds on October 2 & 3 and October 7 & 8 (Fig. 1c and Table 1) allow us to place limits on the troposphere circumpolar wind velocities. From October 2 to October 3 we find that the movement of the cloud is consistent with a velocity of 2 +/- 3 m/s. The cloud on October 7 & 8 is consistent with a velocity of 0 +/- 4 m/s. However, the October 7 & 8 cloud is 160 degrees in longitude away from the cloud observed on October 2 & 3. In order for the cloud of October 2 & 3 to have blown to the position of October 7 & 8, it would have needed to move 6 +/- 1 m/s eastward during the 4 days during which we do not have observations. We find it unlikely that a cloud that was consistent with being relatively stationary in two separate locations in two separate sets of observations would move with such a high velocity between observations, thus the October 2-3 cloud and the 7-8 cloud likely formed separately. The former location of the October 2-3 cloud is visible in images from October 7-8, and no cloud activity is seen at this location, so we know that the October 2-3 cloud has disappeared within 4 days. In addition, the

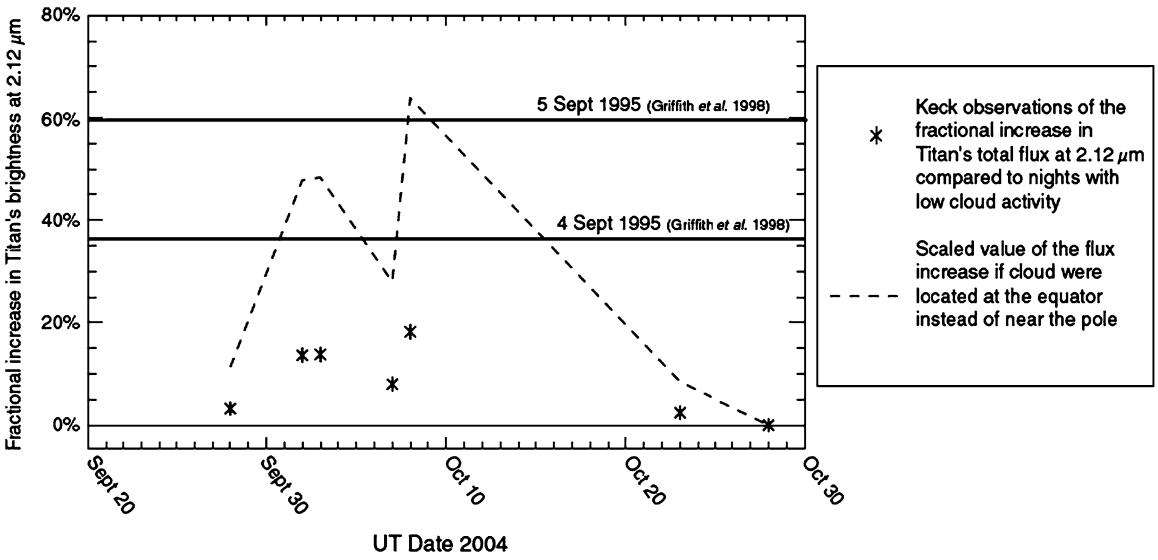

Figure 2.2 a. The fractional increase in Titan's total flux through the cloud filter (2.11-2.14 m) compared to nights with low cloud activity is shown for each night of th outburst. The total flux of Titan increased by nearly 20% on the brightest night of the outburst (8 October 2004). The solid lines show the flux increase in the same wavelength range for the September 1995 cloud outburst of Griffith et al. (1998). We find that the October 2004 storm at the south pole is not as bright by a factor of 3.3. However, the dashed line shows the flux that the October 2004 outburst would have had if it occurred near the equator rather than the pole, estimated by a simple geometric and methane airmass correction. If the October 2004 clouds were at the equator, they would have appeared to be of similar brightness to the September 1995 clouds observed by Griffith et al. (1998).

cloud becomes significantly brighter from October 7th to October 8th (the brightest night of the storm) suggesting that it was actively forming at that location. While the overall period of increased south polar cloud activity lasted for ∼30 days, individual clouds themselves appear to be rapidly forming and dissipating on timescales as short as one earth day. If the clouds are raining out methane, the fast timescales of their dissipation and possible rapid rainout times are consistent with a large raindrop size predicted by Lorenz (1993) and Lorenz & Rennó (2002).

2.5 Discussion

In order to understand Titan's complex meteorology, it is necessary to understand why cloud activity occasionally increases dramatically and why such increases last for weeks. Clouds can form where a parcel of air is lifted sufficiently to become saturated and condensation occurs which releases latent heat. As the parcel is further lifted, sufficient condensation and latent heating occurs to make the parcel warmer than its surroundings and positively buoyant, initiating free moist-convection and convective clouds. The altitude at which a parcel is positively buoyant is called the Level of Free Convection (LFC). Over most of Titan, the dry convective layer near the ground is much lower than LFC so no clouds are formed. The general circulation models of Tokano (2005) predict superadiabatic lapse rates from ∼70-90 S in the current southern summer season. This location corresponds to where the majority of clouds on Titan have been observed (Roe et al. 2002; Brown et al. 2002; Bouchez and Brown 2005) suggesting that there may be sufficient surface heating at these locations to lift parcels to the LFC and instigate convective cloud formation. However, an additional mechanism needs to be invoked to explain the large short-term increase in cloud activity observed in October 2004. We suggest three possible mechanisms that could cause such an increase.

(1) Increased Cloud Condensation Nucleii

Early work suggested that Titan might be lacking in cloud condensation nuclei (CCN) and that the troposphere could therefore be supersaturated in methane (eg. (Courtin et al., 1995; McKay et al., 1997; Samuelson & Mayo, 1997)). A large influx of condensation nuclei into an already saturated or supersaturated parcel above the LFC would cause increased cloud activity and rainout of methane. However, Huygens DISR observations suggested abundant haze particles in the troposphere (Mackwell & Stansbery, 2005) and GCMS observations found no evidence for methane supersaturation (Niemann & The Gcms Experiment Team, 2005). In addition, cloud activity has been regularly observed near Titan's south pole for the past four years suggesting that condensation nuclei have not been lacking. However, addition of extra CCN by some unknown mechanism could cause increased cloud nucleation rates leading to an increase in cloud activity until these particles are rained out.

(2) Localized geologic process leading to surface heating

Increased surface heating from geothermal or volcanic activity near the pole could increase convection leading to a localized increase in cloud activity at that location. If one hot spot were responsible for the large cloud outburst observed, we would expect to see either a continuous source region or a long-lived cloud that moves. Instead, we find large relatively stationary clouds forming in at least two distinct well-separated areas on different sides of the pole. It is unlikely that two separate hot spots near the pole cloud be responsible for the observed clouds. Therefore, increased surface heating is likely not the cause of the observed cloud outburst.

(3) Increased methane humidity at the south pole

Methane injection into Titan's atmosphere must occur in order to compensate for the constant photochemical loss. The current pole-to-pole global circulation would eventually bring this occasionally injected methane toward the south polar region. Increased cloud activity resulting from lowering the LFC by increasing methane humidity would then occur until the additional methane was depleted. Therefore, large cloud events at the south pole could be tied to methane outgasing somewhere on the

surface of Titan. This hypothesis is consistent with large cloud outbursts observed in different seasons of Titan's year. While we cannot rule out some sort of atmospheric wave phenomenon periodically bringing moist air to the pole, the timescales of known terrestrial analog phenomena are at least an order of magnitude longer than the ∼30 day timescale of this outburst (Ingersoll et al., 2005) and predictions of cloud lifetimes caused by horizontal poleward transport of air parcels are an order of magnitude shorter (Barth and Toon 2004). In 1995, we expect that the location of daily clouds and the large cloud outburst observed by Griffith et al. (1998) would have been near the equator because the solar insolation was greatest there and the equator-to-pole cells (Hourdin et al., 1995) would have provided uplift and concentrated occasionally injected methane at the equator.

The Cassini Ta flyby occurred on October 26, 2004 when the cloud outburst was in the process of dissipating. Cassini images from Ta still showed a significant degree of cloud activity at the south pole of Titan compared with other flybys indicating that the outburst had not fully dissipated by October 26th. The Keck image from October 28th, however, shows only a small degree of cloud activity at the pole, consistent with cloud cover of less than 1% observed in most ground-based images of Titan to date. Therefore, images from Ta are particularly interesting because of the rapid dissipation of the clouds that occurred within 48 hours after they were taken.

Ongoing ground-based monitoring campaigns (Schaller et al., 2005) are important for placing these large storms in the broader context of the full range of cloud activity on Titan. The south pole ceased to be the area of maximum solar insolation in July 2005. Over the next several years, as Titan moves away from southern summer solstice, ground-based monitoring campaigns and the numerous Cassini flybys will help to determine how and if the magnitudes and locations of large cloud events will begin to change with season. While apparently infrequent, the fact that large cloud events have been observed in different seasons of Titan's year (near spring equinox in 1995 and post southern summer solstice in 2004) indicates that these large increases

in cloud activity might be a year-round phenomenon on Titan.

Table 2.1 Cloud Details

Image Date (UT)	Planetocentric latitude, longitude of the cloud centers[a]	Velocities of the cloud during the storm (m/s)	Cloud brightness at 2.12 μm[b]
2004 Sep 28	-87^{+3}_{-5}, 96^{+144}_{-35}		0.03 ±0.04
2004 Oct 02	-73 ±3, 337^{+10}_{-8}		0.14 ±0.02
2004 Oct 03	-76 ±3, 321^{+11}_{-14}	$2.2^{+3.4}_{-2.6}$	0.14 ± 0.02
2004 Oct 07	-70 ±3, 163^{+15}_{-13}		0.08 ± 0.01
2004 Oct 08	-72 ±3, 163^{+13}_{-11}	0 ±4	0.18 ± 0.02
2004 Oct 23	-75 ±5, 160^{+18}_{-17}		0.02 ± 0.01

[a]Uncertainties are calculated based on ±0.5 pixels in determining the center of Titan and ±1.5 pixels in determining the centers of the cloud positions

[b]Fractional increase in Titan's total flux at 2.12 μm compared to nights with little to no cloud activity

Bibliography

Barth, E. L. & Toon, O. B. 2004, Geophysics Research Letters, 31, 17

Bouchez, A. H. & Brown, M. E. 2005, Astrophysical Journal, Letters, 618, L53

Bouchez, A. H., Brown, M. E., Schaller, E. L., & Roe, H. G. 2004, in Bulletin of the American Astronomical Society, Vol. 36, Bulletin of the American Astronomical Society, 1117–+

Brown, M. E., Bouchez, A. H., & Griffith, C. A. 2002, Nature, 420, 795

Courtin, R., Gautier, D., & McKay, C. P. 1995, Icarus, 114, 144

Gendron, E., Coustenis, A., Drossart, P., Combes, M., Hirtzig, M., Lacombe, F., Rouan, D., Collin, C., Pau, S., Lagrange, A.-M., Mouillet, D., Rabou, P., Fusco, T., & Zins, G. 2004, Astronomy and Astrophysics, 417, L21

Griffith, C. A., Hall, J. L., & Geballe, T. R. 2000, Science, 290, 509

Griffith, C. A., Owen, T., Miller, G. A., & Geballe, T. 1998, Nature, 395, 575

Griffith, C. A., Penteado, P., Baines, K., Drossart, P., Barnes, J., Bellucci, G., Bibring, J., Brown, R., Buratti, B., Capaccioni, F., Cerroni, P., Clark, R., Combes, M., Coradini, A., Cruikshank, D., Formisano, V., Jaumann, R., Langevin, Y., Matson, D., McCord, T., Mennella, V., Nelson, R., Nicholson, P., Sicardy, B., Sotin, C., Soderblom, L. A., & Kursinski, R. 2005, Science, 310, 474

Hourdin, F., Talagrand, O., Sadourny, R., Courtin, R., Gautier, D., & McKay, C. P. 1995, Icarus, 117, 358

Ingersoll, A. P., Roe, H. G., Schaller, E. L., & Brown, M. E. 2005, in Bulletin of the American Astronomical Society, Vol. 37, Bulletin of the American Astronomical Society, 719–+

Lorenz, R. D. 1993, Planetary Space Science, 41, 647

Lorenz, R. D. & Rennó, N. O. 2002, Geophysics Research Letters, 29, 10

Mackwell, S. & Stansbery, E., eds. 2005, Lunar and Planetary Institute Conference Abstracts, Vol. 36, Aerosol and Cloud Properties at the Huygens Entry Site as Derived from the Descent Imager/Spectral, ed. S. Mackwell & E. Stansbery, 2222–+

McKay, C. P., Martin, S. C., Griffith, C. A., & Keller, R. M. 1997, Icarus, 129, 498

Niemann, H. B. & The Gcms Experiment Team. 2005, in Lunar and Planetary Institute Conference Abstracts, Vol. 36, 36th Annual Lunar and Planetary Science Conference, ed. S. Mackwell & E. Stansbery, 1663–+

Roe, H. G., Bouchez, A. H., Trujillo, C. A., Schaller, E. L., & Brown, M. E. 2005a, Astrophysical Journal, Letters, 618, L49

Roe, H. G., Brown, M. E., Schaller, E. L., Bouchez, A. H., & Trujillo, C. A. 2005b, Science, 310, 477

Roe, H. G., de Pater, I., Macintosh, B. A., & McKay, C. P. 2002, Astrophysical Journal, 581, 1399

Samuelson, R. E. & Mayo, L. A. 1997, Planetary Space Science, 45, 949

Schaller, E. L., Brown, M. E., Roe, H. G., Bouchez, A. H., & Trujillo, C. A. 2005, in Lunar and Planetary Institute Conference Abstracts, Vol. 36, 36th Annual Lunar and Planetary Science Conference, ed. S. Mackwell & E. Stansbery, 1989–+

Tokano, T. 2005, Icarus, 173, 222

Wizinowich, P., Acton, D. S., Shelton, C., Stomski, P., Gathright, J., Ho, K., Lupton, W., Tsubota, K., Lai, O., Max, C., Brase, J., An, J., Avicola, K., Olivier, S., Gavel, D., Macintosh, B., Ghez, A., & Larkin, J. 2000, Publications of the ASP, 112, 315

Chapter 3

Dissipation of Titan's South Polar Clouds

http://apod.nasa.gov/apod/ap990629.html

This chapter has been published in its entirety under the same title by authors E.L. Schaller, M.E. Brown, H.G. Roe, A.H. Bouchez, and C.A. Trujillo in *Icarus*, 2006, Volume 184, pp. 517–523.

3.1 Abstract

Nearly all adaptive optics images of Titan taken between December 2001 and November 2004 showed tropospheric clouds located within 30 degrees of the south pole. We report here on a dissipation of Titan's south polar clouds observed in twenty-nine Keck and Gemini images taken between December 2004 and April 2005. The near complete lack of south polar cloud activity during this time, and subsequent resurgence months later at generally higher latitudes, may be the beginning of seasonal change in Titan's weather. The ∼5 month decrease in cloud activity may also have been caused by methane rainout from a large cloud event in October 2004. Understanding the seasonal evolution of Titan's clouds, and of any precipitation associated with them, is essential for interpreting the geological observations of fluid flow features observed over a wide range of Titan latitudes with the Cassini/Huygens spacecraft.

3.2 Introduction

Data obtained from the Voyager encounters with Saturn's moon Titan first suggested that Titan might support a methane meteorological cycle analogous to Earth's hydrological cycle including methane clouds, rain and oceans (Flasar, 1983; Lunine et al., 1983; Yung et al., 1984). Titan's thick stratospheric haze prevented Voyager cameras from imaging the lower atmosphere and surface to confirm or deny the existence of oceans or clouds. The first images of Titan's surface were taken in the near infrared with the Hubble Space Telescope (Smith et al., 1996). These images revealed large bright and dark regions on Titan's surface that were hypothesized to correspond to continent-like land masses and hydrocarbon oceans respectively.

Arecibo radar observations seemed to confirm the idea that Titan's surface possessed bodies of liquid methane or other hydrocarbons (Campbell et al., 2003). In 12 out of 16 observed locations on Titan's surface, Campbell et al. (2003) saw a specular reflection indicating that Titan was extremely smooth on the scale of centimeters

in these locations. It was expected that data from the Cassini spacecraft would reveal lakes or seas of liquid methane or other hydrocarbons. The Huygens lander was even designed to function if it landed on a liquid surface (Lebreton & Matson, 2002). However, the Huygens landing spot was solid even though it landed in one of the dark areas originally thought to be composed of liquid hydrocarbons (Zarnecki et al., 2005).

Recent Keck observations in the infrared have also found no evidence for specular reflection indicating that Titan is not smooth on the scale of microns (West et al., 2005). The radar and IR observations are consistent if the surface is smooth on centimeter scales but not on micron scales. Such a surface could be formed by evaporite deposits, frozen cryolavas, or deposits of organic haze (West et al., 2005). In addition, the VIMS instrument has found no evidence for specular reflection anywhere it has looked (Brown et al., 2005).

Though Cassini has not found any evidence for liquids currently on the surface, images taken during the Huygens descent provide strong morphological evidence that liquids have flowed across the surface in the past (Lebreton et al., 2005). Huygens descent images revealed incised, river-like channels appearing to empty into a dark flat area. These images force questions about how long ago liquid methane last flowed through these channels. Are Titan's channels similar to ancient valley networks on Mars where water dried up billions of years ago, or does methane still rain down and flow across the surface of Titan today?

The scarcity of impact craters observed by Cassini point to a young surface age. Though Titan's atmosphere screens out impactors that form craters of less than 20 km, the dearth of midsized craters is consistent with a relatively young surface age (Lunine et al., 2005). Though the cratering record can provide constraints on Titan's surface age, in order to begin to answer questions about when and where liquid methane last flowed across the surface of Titan, the most important pieces of available data are observations of Titan's clouds. Understanding Titan's complex

meteorological cycle can provide clues about when it last rained at the Huygens landing site and when it might rain again.

Clouds on Titan were first detected in 1995 by Griffith et al. (1998) via whole disk spectroscopy. On two nights out of 12 that they observed, Griffith et al. (1998) witnessed Titan brightening by up to 200% in regions of Titan's spectrum in which photons penetrated to the troposphere. They found that this dramatic, transient brightening corresponded to cloud cover of ∼7-9% of Titan's disk with a cloud altitude of ∼16 km. While there is some evidence that this cloud was near the equator based on spectral changes from one night to the next, the latitude of the cloud is unknown. Griffith et al. (2000) continued their spectroscopic monitoring of Titan in methane windows and found daily clouds that appeared to vary on the timescales of hours and corresponded to total cloud coverage of ≤1% of Titan's disk.

The first direct detection of clouds on Titan was achieved with the adaptive optics systems on the Keck and Gemini telescopes by Brown et al. (2002) and Roe et al. (2002). These observations also revealed cloud cover of 1% of Titan's disk consistent with the magnitudes of the daily clouds observed spectroscopically by Griffith et al. (2000). Images of Titan's clouds revealed that they were all located within about 30 degrees of the south pole. The location near the pole and the fact that Titan summer solstice occurred in October 2002, led Brown et al. (2002) to propose a convective cloud formation mechanism driven by surface heating due to the increased solar insolation at the south pole. Small (∼1 degree) increases in surface temperature increase the lapse rate sufficiently to instigate moist convection in Titan's usually convectively stable atmosphere (Brown et al. 2002). Brown et al. (2002) predicted that the locations of the clouds should move north with the changing season.

Recent GCM modeling of Titan by Tokano (2005) has predicted that the temperature at the south pole could vary by ∼4 degrees during the course of a Titan year assuming a surface composed of porous icy regolith. Tokano (2005) also mapped locations of convective zones (locations where the lapse rate exceeds the dry adiabat)

near the surface for different seasons. He found superadabatic lapse rates between 50-90S latitude at Ls 270 (southern summer solstice) with the highest values of the lapse rate at the south pole. The locations of Tokano's convective zones are consistent with the observed locations of Titan's clouds which have regularly been observed from ∼60-90 S latitude by ground based observers since 2001 and by Cassini (Bouchez & Brown, 2005; Gendron et al., 2004; Brown et al., 2002; Roe et al., 2002; Porco et al., 2005).

In October 2004 Schaller et al. (2006a) witnessed a brightening of Titan's south polar clouds of comparable magnitude to the large cloud event observed in 1995 by Griffith et al. (1998). This observation indicated that large cloud events occasionally occur during different seasons of Titan's year (southern spring equinox and southern summer solstice). Schaller et al. (2006) suggested that these large cloud events might be caused by methane injection somewhere on the surface of the planet that is then concentrated near the pole via Titan's global circulation.

The four years of adaptive optics observations of Titan comprise less than 1/7 of a full Titan year and have essentially bracketed the period surrounding southern summer solstice (Figure 3.1). However, as of July 2005, the south pole ceased to be the area of maximum solar insolation on Titan. The discovery of streaky, extended clouds at temperate latitudes (∼40 S) in December 2003 was initially thought to be evidence for seasonal change in Titan's cloud activity (Roe et al., 2005a). However, subsequent observations by Roe et al. (2005b) showed that these clouds were clustered in longitude (near 350W) and that due to an odd coincidence of when Titan was observed prior to 2003, there was very little coverage of the side of Titan on which the midlatitude clouds occasionally appear. Roe et al. (2005b) suggested that the strong tie to a particular location on Titan's surface indicated that these clouds form by the release of volatiles or other geologic activity occurring near 40S, 350W. Other authors (Griffith et al., 2005; Rannou et al., 2006) have suggested that the midlatitude clouds form as a result of Titan's global circulation.

In contrast to the simple picture of cloud locations generally following the area of maximum solar insolation, modeling by Rannou et al. (2006) predicts that Titan's tropospheric methane clouds should be present near the south and north poles at nearly all seasons. Their model also predicts sporadic tropical methane clouds occurring at 40 S corresponding to the ascending branch of the troposphere Hadley cell. These clouds should appear at 40 N around the time of northern solstice. They predict that south polar clouds should decrease in frequency in the years following the summer solstice and then reappear after equinox in about 2010. The differences between the Tokano (2005) and Rannou et al. (2006) models may be due to the high value of thermal inertia (2000 $Jm^{-2}s^{-0.5}K^{-1}$) used by Rannou et al. (2006) compared to case 1 of the Tokano (2005) model with a thermal inertia of 335 $Jm^{-2}s^{-.5}K^{-1}$. The high value of thermal inertia does not allow the surface temperature to vary significantly with season which could influence the predicted locations of cloud activity. Another difference between the models is in their treatment of the spectral properties and spatial extent of Titan's stratospheric haze. The aggregate particles and high haze optical depth at the poles used in the Rannou (2006) model may be more realistic. The properties of Titan's stratospheric haze may significantly influence the locations of its tropospheric clouds.

One potential inconsistency with the simple picture of cloud systems following insolation and circulation and support for the Rannou et al. (2006) model comes from early observations of Gibbard et al. (2004) in 1998 near the time of the equinox. At a time when clouds would be expected near the equator in the insolation driven model, they obtained tentative evidence of a cloud near the south pole. Unfortunately, the data were obtained before the days of routine high-resolution adaptive optics imaging and instead had to use the much more difficult technique of speckle interferometry. This technique can introduce artifacts, particularly near sharp edges such as the south pole. The data look tentatively convincing, but it is difficult to assess their reliability. The best resolution of this data point will come over the next few years as we observe

Titan's cloud systems again move through the equinox. If Titan's clouds continue to occur near the south pole even sporadically during equinox, then the simple picture of convective clouds driven by surface heating should be discarded.

Thus far, there is no confirmed evidence for seasonal variation of Titan's clouds. Small, daily clouds have been regularly observed near the south pole since 2001 when adaptive optics observations began. Large cloud events, while infrequent, have been observed to occur in two different seasons, (spring equinox and 2 years post summer solstice). Midlatitude clouds may be caused by surface outgassing and/or may be related to the global circulation (Griffith et al. 2005, Roe et al. 2005b). However, there is no evidence that they are a recent phenomenon (Roe et al. 2005b). We report here on a near-complete disappearance of Titan's south polar clouds observed in twenty-nine Keck and Gemini images taken between December 2004 and April 2005 and comment on the possibility that this decrease and subsequent resurgence of cloud activity at generally higher latitudes could be the start of seasonal change in Titan's cloud activity. These observations will provide the best tests for discriminating between competing models of cloud formation.

3.3 Observations and Results

Titan images presented here come from two long-term Titan monitoring programs carried out on the W.M. Keck 10-m and the Gemini North 8-m telescopes (Table 3.1). Keck images were taken with the facility adaptive optics system and the either the NIRC2 near-infrared camera (Wizinowich et al., 2000) or the imager on the OH Suppressing Infrared Imaging Spectrograph (OSIRIS) (Quirrenbach et al., 2006). Gemini images were acquired with the Altair adaptive optics system and the facility near infrared camera (Herriot et al., 2000; Hodapp et al., 2003).

Keck NIRC2 and Gemini images were taken through three different filters that probe to different levels in Titan's atmosphere. Because the strength of the collision

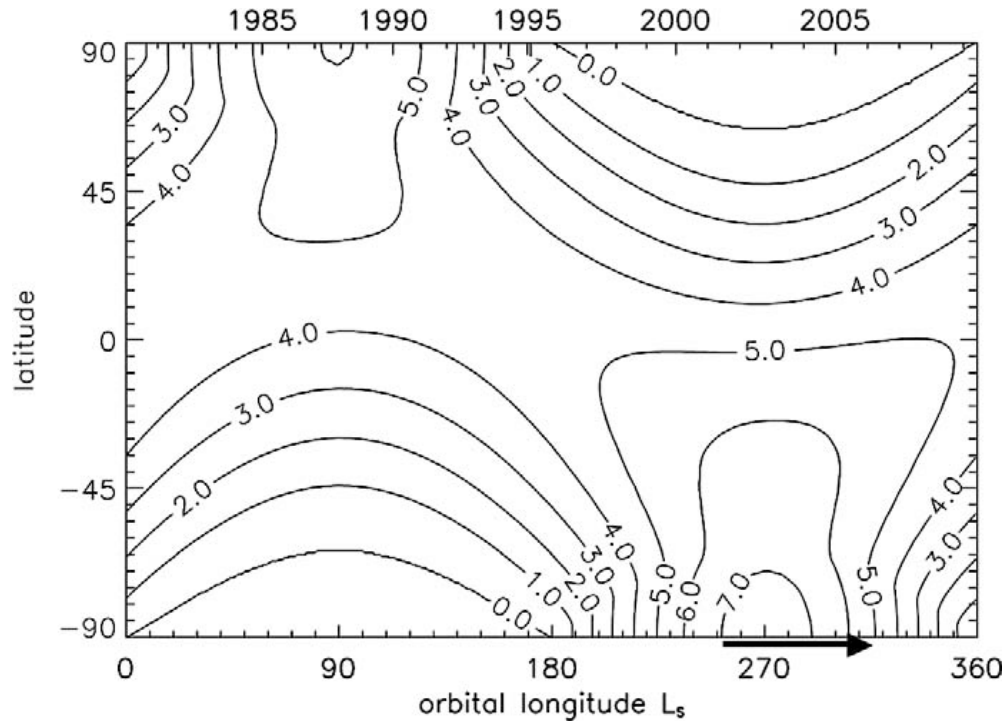

Figure 3.1 Mean daily insolation at the top of Titan's atmosphere vs. latitude and season in units of W/m^2. During most of the four years of adaptive optics observations of Titan's clouds (indicated by the black arrow), the south pole received the maximum daily insolation of anywhere on Titan. In July 2005 the south pole ceased to be the area of maximum solar insolation. The dissipation of Titan's south polar clouds and recent resurgence at higher latitudes may be the first indications of seasonal change in Titan's cloud activity.

induced absorption from methane and H2-N2/N2-N2 depends greatly on wavelength in the near infrared, we are able to probe to different levels in Titan's atmosphere with the use of different filters. Keck NIRC2 images were taken through the K' filter (1.948-2.299 um) that probes to Titan's surface, the H2 (1-0) filter (2.1112-2.1452 um) that probes to ∼10 km altitude (lower troposphere), and the Bγ filter (2.1426-2.1780 um) that probes to ∼50 km altitude (tropopause). Keck OSIRIS images were taken through the Kn2 (2.0381-2.1429 um) and Kn3 (2.1216-2.2297) filters. The Kn2 filter probes to Titan's surface while the Kn3 probes to the troposphere. Gemini images were taken through the K' surface probing filter, the H2 (1-0) troposphere probing filter and the Bγ tropopause probing filter. Titan's clouds are visible in the surface probing filters (though they are often difficult to distinguish from surface features), visible in the troposphere-probing filter, and then generally not visible in the tropopause/stratosphere probing filters indicating that they are located in the troposphere. We use the troposphere probing filters in our analysis of cloud locations.

The Keck and Gemini Titan monitoring programs have yielded 83 individual nights of Titan images from September 2003 to December 2005 (Table 1). We combine our dataset with Titan adaptive optics images from the Palomar 200-inch (previously published in Bouchez and Brown (2005)), and Keck images previously published in Brown et al. (2002) and Roe et al. (2002). The combined dataset yields 100 separate nights spanning the time period from December 2001 through December 2005. Images were flat-fielded, corrected for bad pixels and oriented so that Titan's north pole was aligned with the vertical axis. Cloud locations were measured from a latitude/longitude grid projected onto Titan's disk. Errors in cloud locations are derived from the uncertainty in locating the center of Titan's disk (estimated to be 0.5 pixel) and the uncertainty in locating the centers of the clouds (estimated to be 1 pixel).

Figure 3.2 shows the latitudes of Titan's clouds observed in all images from 2001 to 2005. Also plotted are dates of observations where no clouds were observed. We ignore midlatitude clouds (Roe et al. 2005a & b; Griffith et al. 2005) in this analysis

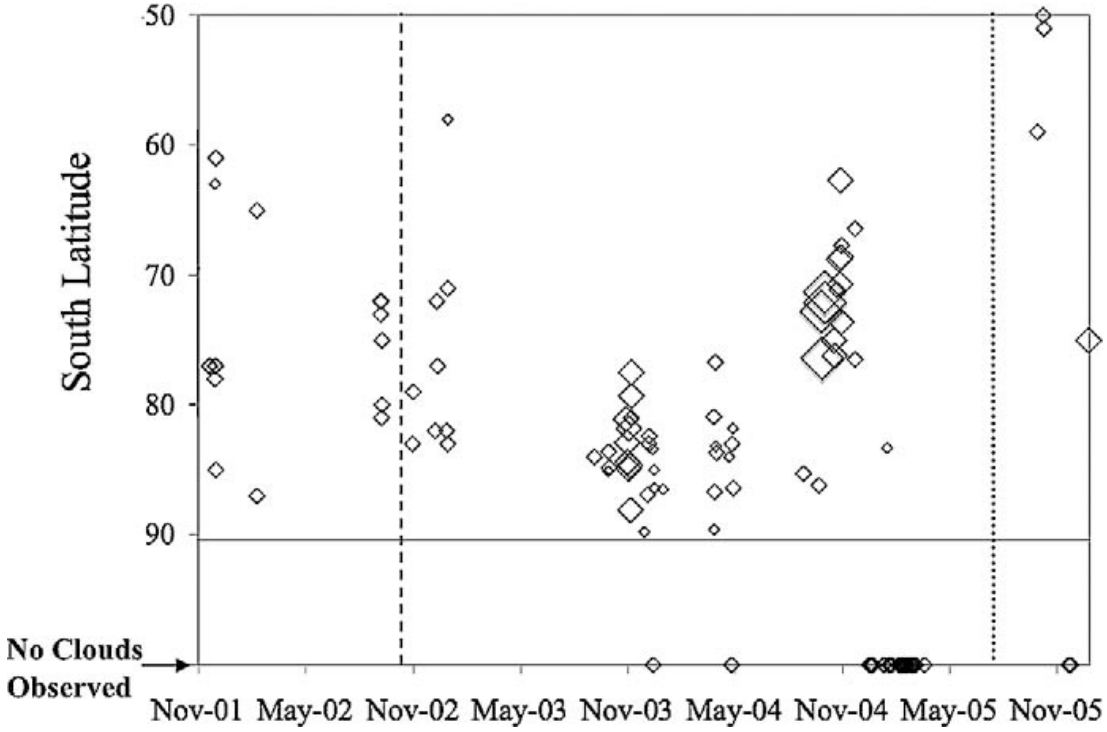

Figure 3.2 Titan cloud locations vs. time. This figure excludes all midlatitude clouds from Roe et al (2005) which are all located near 40 S and are clustered in longitude near 350W. Diamond sizes indicate the relative size of the cloud observed. Dashed line marks Titan southern summer solstice which occurred in October 2002. Dotted line marks July 2005, the time at which when the south pole ceased to be the area of maximum solar insolation on Titan. Before December 2004, clouds were observed within 30 degrees of the south pole in nearly every adaptive optics image of Titan. During the five month period between December 2004 and April 2005 only one image shows even a small amount of cloud activity at the pole. Images taken in the current (2005-2006) Titan apparition show a resurgence of Titan's clouds at the highest latitudes yet seen.

as their formation mechanism may be tied to the surface geography. We find that a cloud or clouds were present between 58-90 S latitude in 62 out of 64 images from December 2001 to November 2004 and most were clustered between 75-90 S. We find no statistically significant trend of cloud latitude with time in images before 2004. We also measured the longitudes of Titan's clouds and found no correlation between longitude with time or with Titan time of day.

In contrast to images taken before December 2004, we found no south polar clouds at all in 28 out of 29 images from December 2004 to April 2005. Clouds with brightnesses of 0.03% and 0.04% of Titan's could have been detected in Keck and Gemini images respectively. The lack of clouds in these images is a striking change in the behavior of Titan's south polar clouds compared with all other previous observations. Figure 3.3 shows the 29 nights of Titan images taken between December 2004 and April 2005 showing the decreased to nonexistent cloud activity at the south pole (only one image has even a small cloud discernable near the pole). Recent images taken in the 2005-2006 Titan apparition show a resurgence of Titan's south polar cloud activity at generally lower latitudes. OSIRIS images from October 9 and October 10 show clouds at 51 and 53 degrees south which is the furthest north these clouds have ever been observed.

3.4 Discussion

The timing of the observed breakup of Titan's south polar cloud system along with the resurgence of clouds at generally lower southern latitudes ($\sim$55 S) is consistent with the timing of the seasonal shift of the location of maximum solar insolation away from the south pole. The timing is also consistent with an expected decrease in south polar cloud activity predicted in the Rannou et al. (2006) model. As of July 2005, the latitude of maximum insolation on the disk moved to 35 degrees south and will continue moving north until it reaches the equator in 2008 and then moves to the

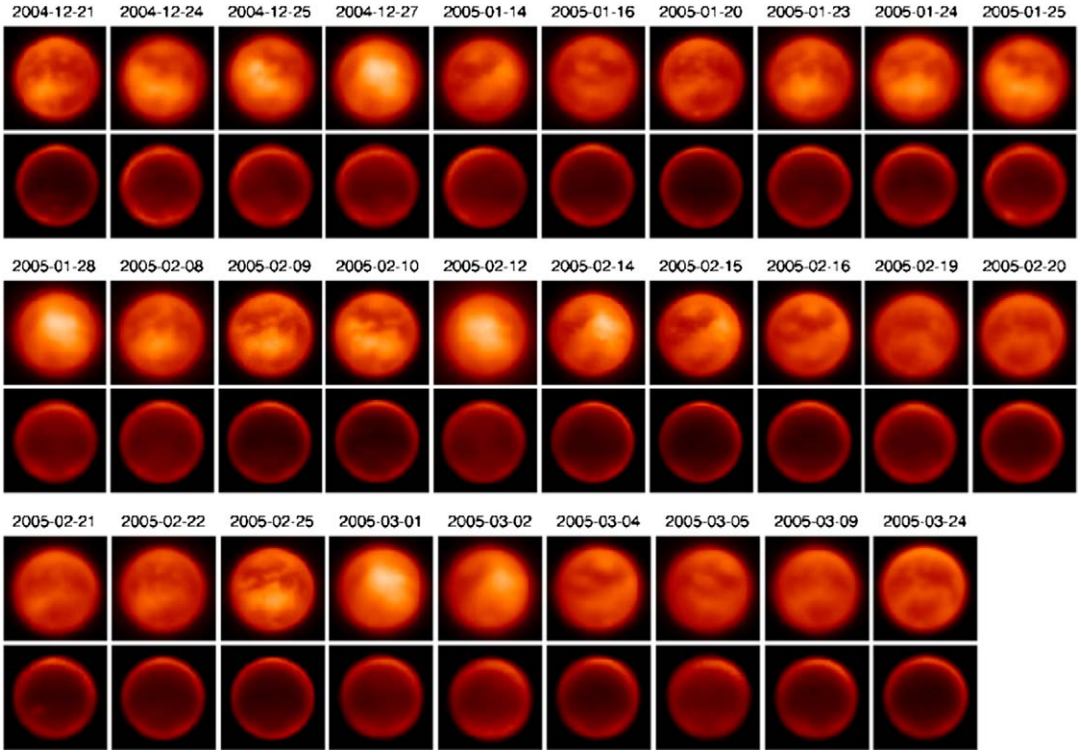

Figure 3.3 Twenty-nine nights of Titan images taken with the Keck and Gemini adaptive optics systems. The top set of images are taken through the K' (surface probing) filter, while the second set of images are taken through the H2 (1-0) (troposphere probing) filter. All images show extremely low to nonexistent cloud activity near the south pole compared with all previous images (see Bouchez and Brown 2005; Brown et al. 2002; Roe et al. 2002; Schaller et al. 2006). In Keck and Gemini images we could have detected point source clouds with brightnesses of 0.03% and 0.04% of Titan's total flux. In order to confirm a cloud detection, we required it to be observable in both the Knd H2 filters.

north pole. Subsequent observations of Titan over the next several years may continue to show decreased to nonexistent cloud activity near the south pole. However, if cloud activity continues near the south pole and is observed near the north pole significantly before northern summer solstice, then the simple picture of cloud activity following the insolation will need to be discarded. Frequent equatorial clouds after 2008 and a lack of south polar clouds would provide support for the insolation driven cloud model. The latitudes of Titan's clouds with season are likely controlled by complex interplay between insolation and uplift from global circulation, and may behave in complicated ways as the season changes.

In addition to possible seasonal change, periods of low cloud activity on Titan might also be explained by the fact that they generally occur following periods of increased cloud activity. The ∼5 month near disappearance of Titan's clouds observed from November 2004 to at least April 2005 occurred immediately following the largest cloud outburst ever observed. The brightness of Titan's south polar clouds increased by over 15 times their typical values for approximately 30 days in October 2004 (Schaller et al. 2006). In addition, one of only two times before December 2004 when there were no clouds observed, occurred following brighter clouds observed in November 2003 (Figure 2). The lack of cloud activity following large cloud events might indicate that these large events are associated with methane rainout, the evaporation of which could cool the atmosphere or surface and inhibit subsequent convection for periods of weeks to months. In addition, rainout could have washed out cloud condensation nuclei thereby inhibiting cloud formation. It is likely that the low level of cloud activity observed from December 2004 to April 2005 was caused by both the large cloud outburst of October 2004 and by the beginnings of seasonal change caused by the changing insolation and circulation.

While Cassini has found no specular evidence for liquids on Titan's surface, the geometry of the flybys have prevented looking for specular points in the far southern latitudes -exactly the location where liquids, if they do currently exist on the surface,

are most likely to be found in the present season. The recent discovery of the dark lake-like feature in ISS images (Turtle et al., 2005), and the detection of a shoreline-like feature in RADAR images (Lopes et al., 2005) near the south pole suggests that liquid methane might currently exist on the surface of Titan. The locations of liquids on the surface may shift from pole to pole as a result of rain out from the clouds that may move according to the changing seasons or may remain near the south pole according to the Rannou et al. (2006) model. Titan observations over the next few years will reveal how cloud activity changes with season and will help to clarify and interpret when and how the fluvial surface features seen in Huygens descent images were formed.

Table 3.1. Titan Cloud Observations

UT Date	Telescope	Cloud Latitude
2003 Sep 17	Keck NIRC2	84 ±2
2003 Oct 10	Keck NIRC2	85 ±3
2003 Oct 11	Keck NIRC2	84 ±5
2003 Oct 12	Keck NIRC2	85 ±4
2003 Nov 09	Keck NIRC2	81 ±2
2003 Nov 11	Keck NIRC2	83 ±2
2003 Nov 12	Keck NIRC2	84 ±2
2003 Nov 13	Keck NIRC2	85 ±3
2003 Nov 14	Keck NIRC2	82 ±3
2003 Nov 15	Gemini	85 ±5
2003 Nov 17	Gemini	88 ±3
2003 Nov 18	Keck NIRC2	79 ±2
		78 ±2
2003 Dec 10	Keck NIRC2	90 ±4
2003 Dec 15	Keck NIRC2	87 ±4
2003 Dec 17	Keck NIRC2	83 ±4
2003 Dec 18	Keck NIRC2	82 ±3
2003 Dec 24	Keck NIRC2	83 ±4
2003 Dec 25	Keck NIRC2	none
2003 Dec 26	Keck NIRC2	85 ±3
2003 Dec 27	Keck NIRC2	86 ±3
2004 Jan 10	Keck NIRC2	87 ±4
2004 Apr 04	Gemini	81 ±6
2004 Apr 05	Gemini	90 ±7
2004 Apr 06	Gemini	87 ±6
2004 Apr 07	Gemini	77 ±7
2004 Apr 08	Gemini	83 ±5
2004 Apr 09	Gemini	84 ±6
2004 Apr 30	Gemini	84 ±3
2004 May 04	Gemini	None
2004 May 05	Gemini	83 ±5
2004 May 06	Gemini	82 ±4
2004 May 07	Gemini	86 ±5
2004 Sep 02	Keck NIRC2	85 ±3
2004 Sep 28	Keck NIRC2	86 ±3

Table 3.1 (cont'd)

UT Date	Telescope	Cloud Latitude
2004 Oct 02	Keck NIRC2	73 ±3
2004 Oct 03	Keck NIRC2	76 ±3
2004 Oct 07	Keck NIRC2	71 ±2
2004 Oct 08	Keck NIRC2	72 ±3
2004 Oct 23	Keck NIRC2	75 ±2
2004 Oct 24	Gemini	76 ±6
2004 Oct 28	Keck NIRC2	71 ±2
2004 Nov 01	Gemini	69 ±5
2004 Nov 02	Gemini	71 ±2
2004 Nov 03	Keck NIRC2	69 ±2
		63 ±3
2004 Nov 04	Gemini	74 ±4
2004 Nov 05	Gemini	68 ±3
2004 Nov 27	Keck NIRC2	77 ±3
		66 ±3
2004 Dec 21	Gemini	None
2004 Dec 24	Gemini	None
2004 Dec 25	Gemini	None
2004 Dec 27	Gemini	None
2005 Jan 14	Keck NIRC2	None
2005 Jan 16	Gemini	None
2005 Jan 20	Keck NIRC2	83 ±2
2005 Jan 23	Gemini	None
2005 Jan 24	Gemini	None
2005 Jan 25	Gemini	None
2005 Jan 28	Gemini	None
2005 Feb 08	Gemini	None
2005 Feb 09	Gemini	None
2005 Feb 10	Gemini	None
2005 Feb 12	Gemini	None
2005 Feb 14	Keck NIRC2	None
2005 Feb 15	Keck NIRC2	None
2005 Feb 16	Gemini	None
2005 Feb 19	Gemini	None
2005 Feb 20	Gemini	None

Table 3.1 (cont'd)

UT Date	Telescope	Cloud Latitude
2005 Feb 21	Gemini	None
2005 Feb 22	Gemini	None
2005 Feb 25	Gemini	None
2005 Mar 01	Gemini	None
2005 Mar 02	Gemini	None
2005 Mar 04	Gemini	None
2005 Mar 05	Gemini	None
2005 Mar 09	Gemini	None
2005 Mar 24	Gemini	None
2005 Sep 29	Keck NIRC2	59 $\pm$2
2005 Oct 09	Keck OSIRIS	50 $\pm$3
2005 Oct 10	Keck OSIRIS	51 $\pm$3
2005 Nov 21	Keck OSIRIS	None
2005 Nov 22	Keck OSIRIS	None
2005 Nov 24	Keck OSIRIS	None
2005 Dec 24	Keck NIRC2	75 $\pm$2

Bibliography

Bouchez, A. H. & Brown, M. E. 2005, Astrophysical Journal, Letters, 618, L53

Brown, M. E., Bouchez, A. H., & Griffith, C. A. 2002, Nature, 420, 795

Brown, R., Baines, K., Bellucci, G., Buratti, B., Capaccioni, F., Cerroni, P., Clark, R., Combes, M., Coradini, A., Cruikshank, D., Drossart, P., Formisano, V., Jaumann, R., Langevin, Y., Matson, D., McCord, T., Mennella, V., Nelson, R., Nicholson, P., Sicardy, B., Sotin, C., Soderblom, L., Barnes, J., Griffith, C., Hansen, G., Hibbitts, K., & Showalter, M. 2005, in Bulletin of the American Astronomical Society, Vol. 37, Bulletin of the American Astronomical Society, 631–+

Campbell, D. B., Black, G. J., Carter, L. M., & Ostro, S. J. 2003, Science, 302, 431

Flasar, F. M. 1983, Science, 221, 55

Gendron, E., Coustenis, A., Drossart, P., Combes, M., Hirtzig, M., Lacombe, F., Rouan, D., Collin, C., Pau, S., Lagrange, A.-M., Mouillet, D., Rabou, P., Fusco, T., & Zins, G. 2004, Astronomy and Astrophysics, 417, L21

Gibbard, S. G., Macintosh, B., Gavel, D., Max, C. E., de Pater, I., Roe, H. G., Ghez, A. M., Young, E. F., & McKay, C. P. 2004, Icarus, 169, 429

Griffith, C. A., Hall, J. L., & Geballe, T. R. 2000, Science, 290, 509

Griffith, C. A., Owen, T., Miller, G. A., & Geballe, T. 1998, Nature, 395, 575

Griffith, C. A., Penteado, P., Baines, K., Drossart, P., Barnes, J., Bellucci, G., Bibring, J., Brown, R., Buratti, B., Capaccioni, F., Cerroni, P., Clark, R., Combes, M., Coradini, A., Cruikshank, D., Formisano, V., Jaumann, R., Langevin, Y., Matson, D., McCord, T., Mennella, V., Nelson, R., Nicholson, P., Sicardy, B., Sotin, C., Soderblom, L. A., & Kursinski, R. 2005, Science, 310, 474

Herriot, G., Morris, S., Anthony, A., Derdall, D., Duncan, D., Dunn, J., Ebbers, A. W., Fletcher, J. M., Hardy, T., Leckie, B., Mirza, A., Morbey, C. L., Pfleger, M., Roberts, S., Shott, P., Smith, M., Saddlemyer, L. K., Sebesta, J., Szeto, K., Wooff, R., Windels, W., & Veran, J.-P. 2000, in Presented at the Society of Photo-Optical Instrumentation Engineers (SPIE) Conference, Vol. 4007, Proc. SPIE Vol. 4007, p. 115-125, Adaptive Optical Systems Technology, Peter L. Wizinowich; Ed., ed. P. L. Wizinowich, 115–125

Hodapp, K. W., Jensen, J. B., Irwin, E. M., Yamada, H., Chung, R., Fletcher, K., Robertson, L., Hora, J. L., Simons, D. A., Mays, W., Nolan, R., Bec, M., Merrill, M., & Fowler, A. M. 2003, Publications of the ASP, 115, 1388

Lebreton, J.-P. & Matson, D. L. 2002, Space Science Reviews, 104, 59

Lebreton, J.-P., Witasse, O., Sollazzo, C., Blancquaert, T., Couzin, P., Schipper, A.-M., Jones, J. B., Matson, D. L., Gurvits, L. I., Atkinson, D. H., Kazeminejad, B., & Pérez-Ayúcar, M. 2005, Nature, 438, 758

Lopes, R. M., Stofan, E., Elachi, C., Kirk, R., Lorenz, R., Lunine, J., Mitchell, K. L., Ori, G. G., Paganelli, F., Soderblom, L., Wall, S., & Wood, C. 2005, AGU Fall Meeting Abstracts, A2+

Lunine, J., Artemieva, N. A., Lorenz, R. D., & Flamini, E. 2005, in Lunar and Planetary Institute Conference Abstracts, Vol. 36, 36th Annual Lunar and Planetary Science Conference, ed. S. Mackwell & E. Stansbery, 1504–+

Lunine, J. I., Stevenson, D. J., & Yung, Y. L. 1983, Science, 222, 1229

Porco, C. C., Baker, E., Barbara, J., Beurle, K., Brahic, A., Burns, J. A., Charnoz, S., Cooper, N., Dawson, D. D., Del Genio, A. D., Denk, T., Dones, L., Dyudina, U., Evans, M. W., Fussner, S., Giese, B., Grazier, K., Helfenstein, P., Ingersoll, A. P., Jacobson, R. A., Johnson, T. V., McEwen, A., Murray, C. D., Neukum, G., Owen, W. M., Perry, J., Roatsch, T., Spitale, J., Squyres, S., Thomas, P., Tiscareno, M., Turtle, E. P., Vasavada, A. R., Veverka, J., Wagner, R., & West, R. 2005, Nature, 434, 159

Quirrenbach, A., Larkin, J., Barczys, M., Gasaway, T., Iserlohe, C., Krabbe, A., McElwain, M., Song, I., Weiss, J., & Wright, S. 2006, New Astronomy Review, 49, 639

Rannou, P., Montmessin, F., Hourdin, F., & Lebonnois, S. 2006, Science, 311, 201

Roe, H. G., Bouchez, A. H., Trujillo, C. A., Schaller, E. L., & Brown, M. E. 2005a, Astrophysical Journal, Letters, 618, L49

Roe, H. G., Brown, M. E., Schaller, E. L., Bouchez, A. H., & Trujillo, C. A. 2005b, Science, 310, 477

Roe, H. G., de Pater, I., Macintosh, B. A., & McKay, C. P. 2002, Astrophysical Journal, 581, 1399

Schaller, E. L., Brown, M. E., Roe, H. G., & Bouchez, A. H. 2006, Icarus, 182, 224

Smith, P. H., Lemmon, M. T., Lorenz, R. D., Sromovsky, L. A., Caldwell, J. J., & Allison, M. D. 1996, Icarus, 119, 336

Tokano, T. 2005, Icarus, 173, 222

Turtle, E. P., Barnes, J., Buratti, B. J., Collins, G., Fussner, S., Lopes, R., Lorenz, R. D., Lunine, J. I., McCord, T. B., McEwen, A. S., Nelson, R., Perry, J., Porco, C. C., Soderblom, L., Sotin, C., & Wall, S. D. 2005, AGU Fall Meeting Abstracts, A1+

West, R. A., Brown, M. E., Salinas, S. V., Bouchez, A. H., & Roe, H. G. 2005, Nature, 436, 670

Wizinowich, P., Acton, D. S., Shelton, C., Stomski, P., Gathright, J., Ho, K., Lupton, W., Tsubota, K., Lai, O., Max, C., Brase, J., An, J., Avicola, K., Olivier, S., Gavel, D., Macintosh, B., Ghez, A., & Larkin, J. 2000, Publications of the ASP, 112, 315

Yung, Y. L., Allen, M., & Pinto, J. P. 1984, Astrophysical Journal, Supplement, 55, 465

Zarnecki, J. C., Leese, M. R., Hathi, B., Ball, A. J., Hagermann, A., Towner, M. C., Lorenz, R. D., McDonnell, J. A. M., Green, S. F., Patel, M. R., Ringrose, T. J., Rosenberg, P. D., Atkinson, K. R., Paton, M. D., Banaszkiewicz, M., Clark, B. C.,

Ferri, F., Fulchignoni, M., Ghafoor, N. A. L., Kargl, G., Svedhem, H., Delderfield, J., Grande, M., Parker, D. J., Challenor, P. G., & Geake, J. E. 2005, Nature, 438, 792

Chapter 4

Seasonal Change on Titan Observed with IRTF/SpeX

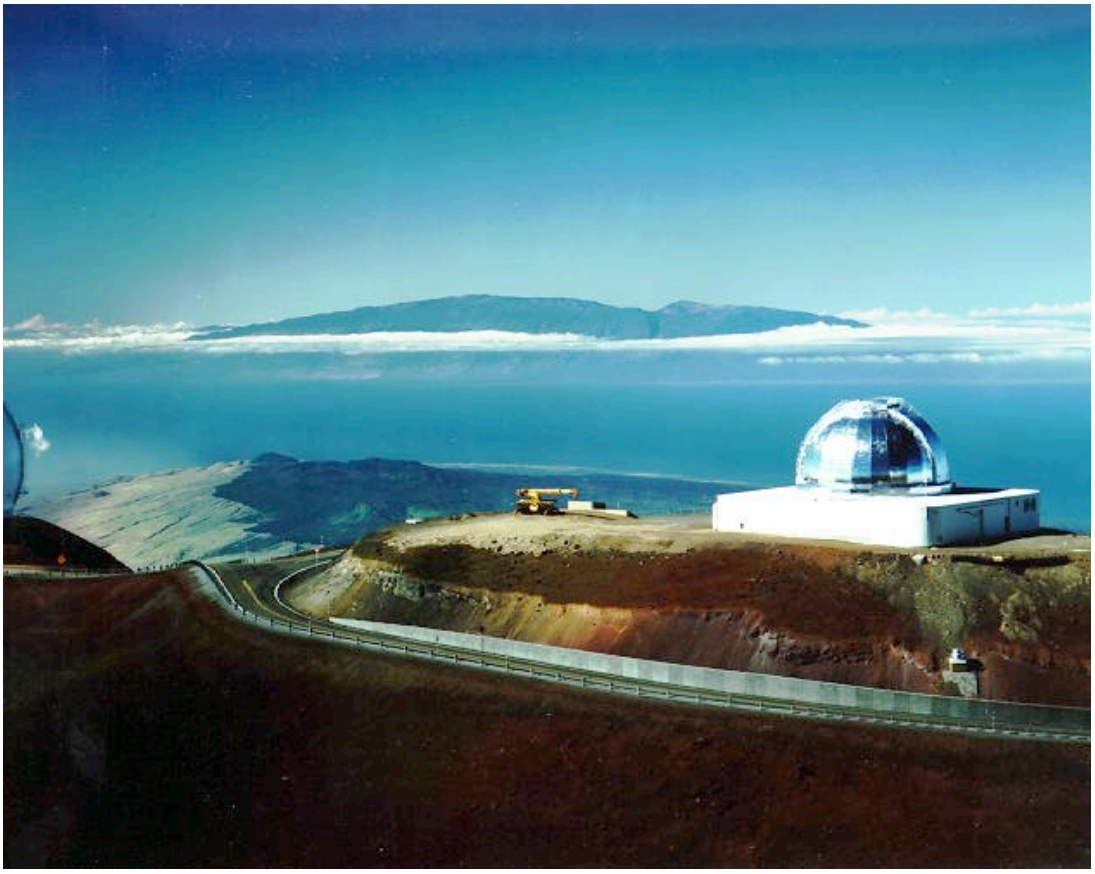

http://irtfweb.ifa.hawaii.edu/images/telescope/irtfmaui.jpg

This chapter will be submitted to Icarus with authors E.L. Schaller, M.E. Brown, H.G. Roe and M. Adamkovics

4.1 Abstract

We obtained a 0.8-2.4 micron whole-disk spectrum of Titan on 138 nights between February 2006 and January 2008 with SpeX at the NASA Infrared Telescope Facility. These spectra allow us to probe Titan's surface and troposphere at 6 distinct low opacity window regions in the near infrared. We observe a seasonal difference in the frequency and brightness of Titan's tropospheric clouds during the present season (3.5-1.5 Earth years pre vernal equinox) compared with previous seasons Titan has been observed (autumnal equinox and northern winter solstice) These data allow us to constrain the total cloud coverage of Titan's disk on 87% nights to be less than 0.15%. On the 13% of nights on which cloud activity was detected, it covered less than 0.4% of Titan's disk at altitudes of 30 km and did not preferentially occur at any particular sub-solar longitude. In addition to providing insight into the long and short-term tropospheric cloud evolution on Titan, these data allow us to independently constrain the amount of the surface flux that penetrates at a given wavelength from 0.8-2.4 microns. Using the combined dataset, we are also able to search for ices with absorption features in the surface-penetrating regions. We place an upper limit of 5% on the fractional coverage of CO_2 ice on Titan's surface.

4.2 Introduction

Titan provides us with a unique laboratory in which to study a hydrological cycle on a planet other than Earth with a different condensable species (methane on Titan, water on Earth). While the presence of Titan's methane meteorological cycle is now well established, a fundamental understanding of the dynamics of Titan's weather including the frequencies, locations, and altitudes of Titan's tropospheric clouds and how these attributes change over Titan's 29.7-year-long seasonal cycle remains unknown. Understanding Titan's hydrological cycle is vital for determining the formation mechanisms of fluvial surface features such as lakes in the north polar regions (Stofan et al.,

2007; Lorenz et al., 2008) and channels near the equator (Soderblom et al., 2007) that have been observed by Cassini/Huygens.

Tropospheric clouds were first observed in 1995 via near-infrared whole disk spectroscopy on UKIRT by Griffith et al. (1998). Griffith et al. (1998) found that tropospheric clouds caused Titan to become brighter in methane windows (where photons penetrate to the surface and lower atmosphere) while staying the same brightness in methane absorption bands. Titan's surface features (such as the large Xanadu feature) also cause brightness variations in these windows but they repeat with phase. By measuring Titan's brightness on the wings of these methane windows (where Titan is moderately opaque and photons penetrate to Titan's troposphere), Griffith et al. (1998) were able to detect variable tropospheric clouds. Spectra covering these wavelengths of low, moderate, and high opacity along with radiative transfer modeling were used to determine cloud heights and total percent cloud coverage of Titan's disk (Griffith et al., 1998, 2000). Tropospheric clouds were detected in nearly all observations, were generally found to cover approximately 0.5% of Titan's disk, and varied on timescales of days and even hours. In addition, in two observations in September 1995, Titan's clouds brightened considerably, covering between 5-7% of its disk.

The first direct detection of Titan's clouds was achieved with the Keck adaptive optics system by Brown et al. (2002) and Roe et al. (2002). From 2001-2004, variable tropospheric clouds were regularly observed near Titan's south pole in adaptive optics images (Bouchez & Brown, 2005; Schaller et al., 2006b). Images taken through the H2(1-0) filter (2.11-2.14 microns) were found to be particularly useful for detecting Titan's clouds, as this filter probes one of the wavelength regions where the moderate opacity causes most of the surface features to be invisible but tropospheric clouds to clearly stand out. The tropospheric clouds observed in Keck, Gemini, and Palomar adaptive optics images typically contributed about 0.5-1% of the total brightness of Titan's disk at 2 microns and were generally found within 20 degrees of the south pole (Brown et al., 2002; Bouchez & Brown, 2005). However, for approximately one

month in October 2004, they increased in brightness to coverages comparable to the 1995 event witnessed by Griffith et al. (1998) (Schaller et al., 2006a).

In addition to the south polar clouds, Roe et al. (2005a,b) and Griffith et al. (2005) also observed clouds at southern midlatitudes (40 S). The streaky, extended morphologies of these clouds were different from the south polar clouds that generally appeared as point sources. The fact that these clouds were clustered in longitude as well as latitude, lead Roe et al. (2005b) to suggest that they were geographically controlled (either due to volcanic outgassing of methane, orography, or other factors). Griffith et al. (2005), who also observed these midlatitude clouds in Cassini images but did not observe a longitude clustering, suggested that their presence at 40 S was related to the changing general circulation patterns supported by the GCM models of Rannou et al. (2006).

Adaptive optics images taken between 2005 and the present have shown that Titan's south polar cloud activity has markedly decreased. Though Cassini still occasionally observes small clouds (Buratti, personal comm.), it is now rare ($\sim$10%) to observe tropospheric cloud activity from the ground in adaptive optics images. In contrast, between 2001- 2005, cloud activity was observed in 97% of adaptive optics images (Schaller et al., 2006b; Bouchez & Brown, 2005). Observations from late 2005 have also shown a hint of cloud activity moving northward (Schaller et al., 2006b) as Titan's season changed from southern solstice (October 2002) and is moving toward vernal equinox (August 2009).

In this paper, we present data from a frequent Titan monitoring program begun at the NASA Infrared Telescope Facility which encompasses two years of observations. These observations allow us to detect tropospheric cloud activity and also reveal fundamental properties of Titan's atmosphere and surface.

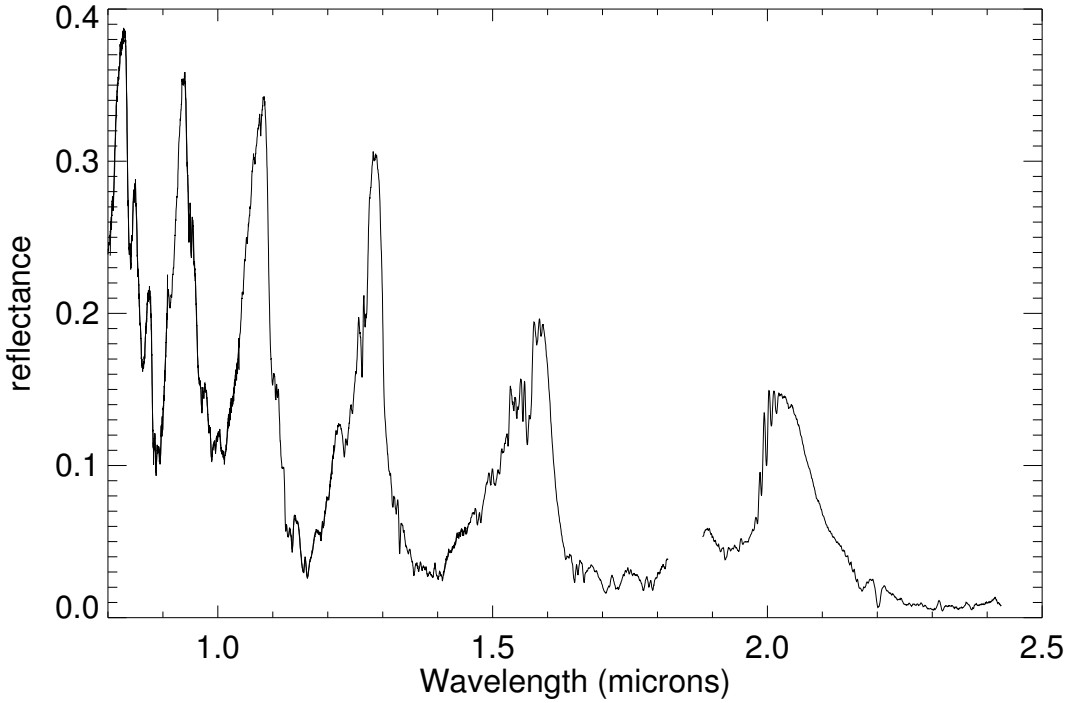

Figure 4.1 Near-Infrared reflectance spectrum of Titan taken with SpeX at the NASA Infrared Telescope Facility on 2008-Jan-04 with a resolution (R∼375).

4.3 Observations

In February 2006 we began our frequent Titan spectral monitoring program with the NASA Infrared Telescope Facility (IRTF). We obtained a near infrared spectrum of Titan with SpeX, the facility visible-near infrared spectrograph (Rayner et al., 2003) on 138 nights from February 2006 to January 2008 (Table 4.1). Observations were taken in the short cross-dispersed (SXD) mode with a 1.6 arcsecond slit. The total spectral range covered was 0.8 to 2.4 microns in 6 orders with a spectral resolution of 375.

On each night, we observed Titan for a total of three minutes of integration time (3 nod pairs of 30 seconds each) while guiding on Titan with the slit guider camera. The slit was oriented in the N/S direction. We performed similar observations of nearby a

G dwarf star (3 nod pairs of 15 seconds). From February 2006 through June 2007 this star was HD 77730 (a G2V) and from October 2007 to January 2008 it was HD 89307 (a G0V). Observations of both stars on several nights allowed us to calibrate the data taken with different stars relative to each other. Titan and the reference star were observed so as to minimize the airmass difference between them (the object with the lower right ascension was observed first). The median difference in airmass between Titan and the star was 0.04 and on only two occasions did it exceed 0.2 (Oct-03-2006 and June-08-2007) In addition, Titan's median airmass was 1.07 and only exceeded 2 airmasses on the dates mentioned above (Table 4.1). Including slewing to Titan and internal calibrations (10 flats and an arc lamp) the total time needed to perform these observations was generally under 20 minutes. Spectral data reduction was performed using standard methods employing the SpeXtool version 3.4 package (Cushing et al., 2004). The six Titan and six star spectra were medianed and the combined Titan spectrum was divided by the combined star spectrum to eliminate telluric features. On clear nights, our 3-minute reduced spectra had a signal-to-noise of approximately 350 per pixel in the 2-2.2 micron region (the wavelength region of particular interest for measuring Titan's tropospheric clouds).

4.4 Results

4.4.1 Lightcurves

The 138 spectra of Titan centered at a variety of Titan longitudes (Figures 4.2, 4.3) provide us with a unique a posteriori method for determining the degree to which photons from the surface penetrate at a given wavelength. Titan's large surface albedo variations with phase provide us with a convenient marker with which to determine the contribution of the surface to Titan's albedo at a given wavelength. This degree to which photons from the surface are able to penetrate at a given wavelength is related to the methane opacity and vertical distribution of aerosols and can be used

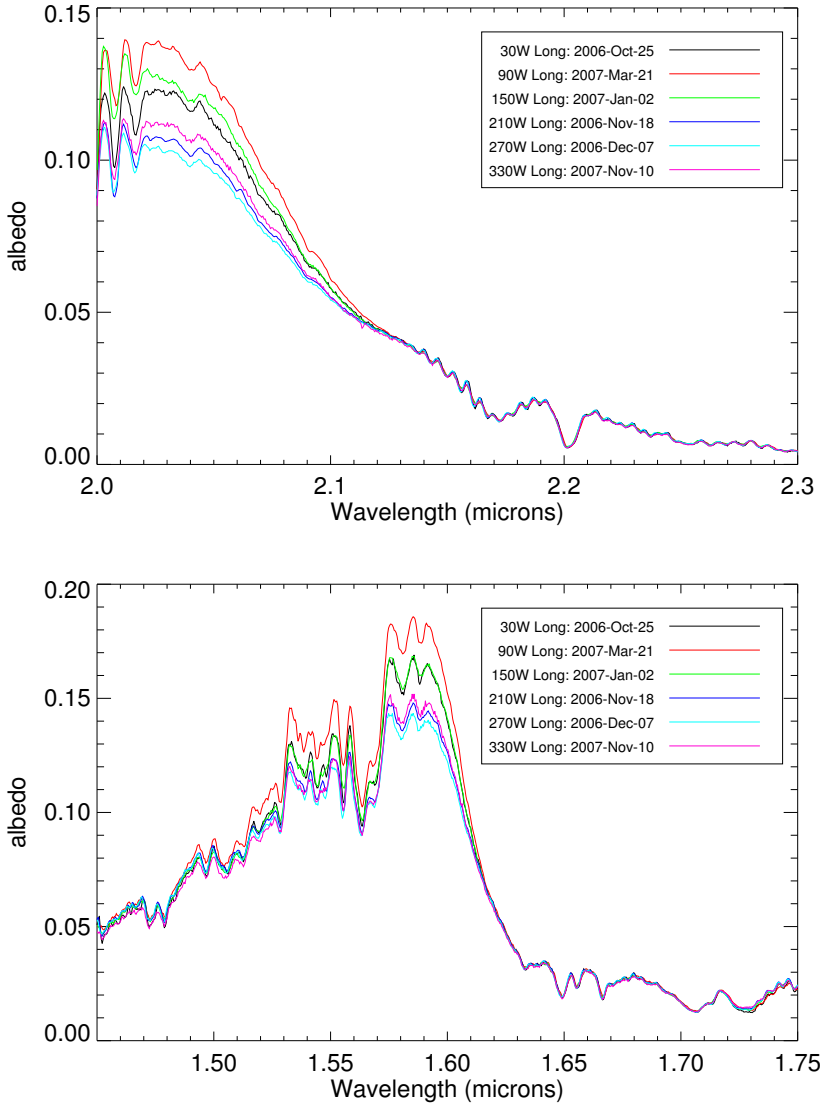

Figure 4.2 Spectra taken at different Titan phases covering the methane window regions in the H and K bands. The spectra lie on top of each other in the high opacity regions (where photons only penetrate to the stratosphere) and differ in low opacity regions (where photons penetrate to the surface and lower atmosphere). The wavelengths at which the spectra deviate from each other, as well as the magnitude of the deviations, allow us to determine if variable tropospheric clouds are present on a given night (see also Figure 4.5).

to constrain radiative transfer models of Titan's atmosphere. Since 1993, it has been known that Titan's surface is brightest at approximately 110W longitude. Cassini and ground-based observers with adaptive optics have shown that this bright region is a continent-sized feature now known as Xanadu. In Figure 4.2 we show H and K band spectra of Titan taken at different central Titan sub-solar longitudes. Each spectrum was normalized to a known high opacity region of Titan's spectrum (2.2-2.25 microns) where photons penetrate only to the upper stratosphere. We expect that that Titan's flux at this wavelength range should stay relatively constant during our observation period. Spectra taken on nights with different central longitudes show similar albedos in wavelength regions that penetrate to Titan's stratosphere but have different albedos in the surface penetrating regions. The albedos in surface penetrating wavelength ranges are correlated in H and K.

Using all 138 nights of data taken with different central longitudes over the course of Titan's 16-day rotation period, we can construct lightcurves at a variety of wavelengths. Figure 4.3 shows four Titan K-band lightcurves. The amplitude of the lightcurve is strongest at 2.02 microns where methane opacity is low and photons can penetrate to Titan's surface. Increasing in wavelength through the K-band, the amplitude of Titan's lightcurve decreases as methane opacity increases. Individual deviations from the lightcurve (best observed in Figure 4.3c) are caused by reflective layers above the surface (clouds) and will be discussed in detail in section 4.4.2. In order to determine the degree to which photons from the surface penetrated at a given wavelength, we measured the amplitude of the lightcurve in 0.0075 micron wavelength bins from 0.8-2.4 microns (Figure 4.4). The amplitudes of the resulting lightcurves with wavelength reveal the presence of 6 distinct window regions in the near-infrared at 0.8, 0.95, 1.05, 1.27, 1.6, and 2 microns where the surface is visible. The 2 micron window is strongest with a surface lightcurve magnitude of approximately 15%.

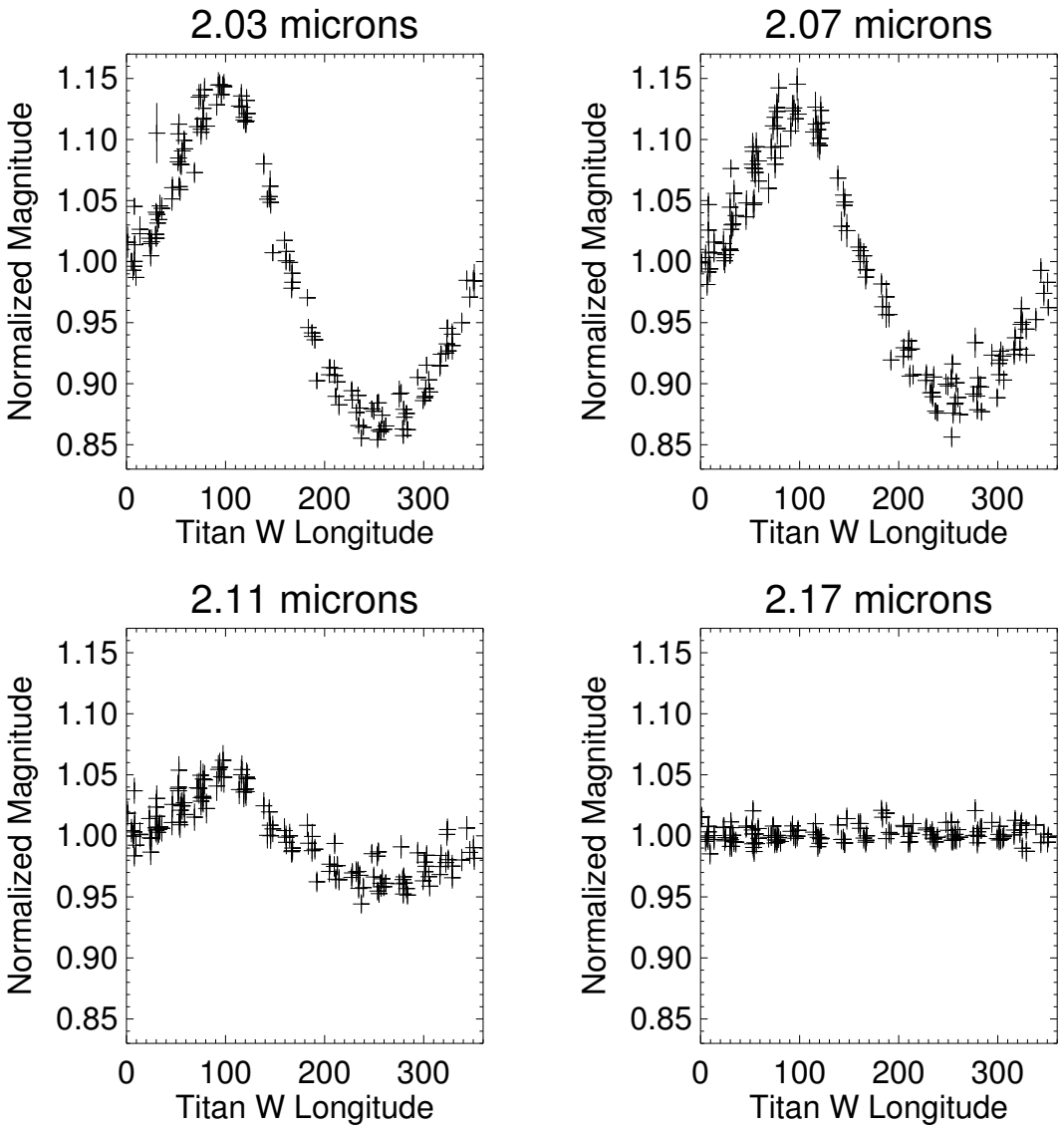

Figure 4.3 K-band lightcurves. The normalized flux at a given wavelength for each of the 138 nights of observations is plotted vs. the Titan central longitude. The magnitude of the lightcurve is greatest near 2.02 microns and decreases with progressively longer wavelengths as Titan's opacity increases.

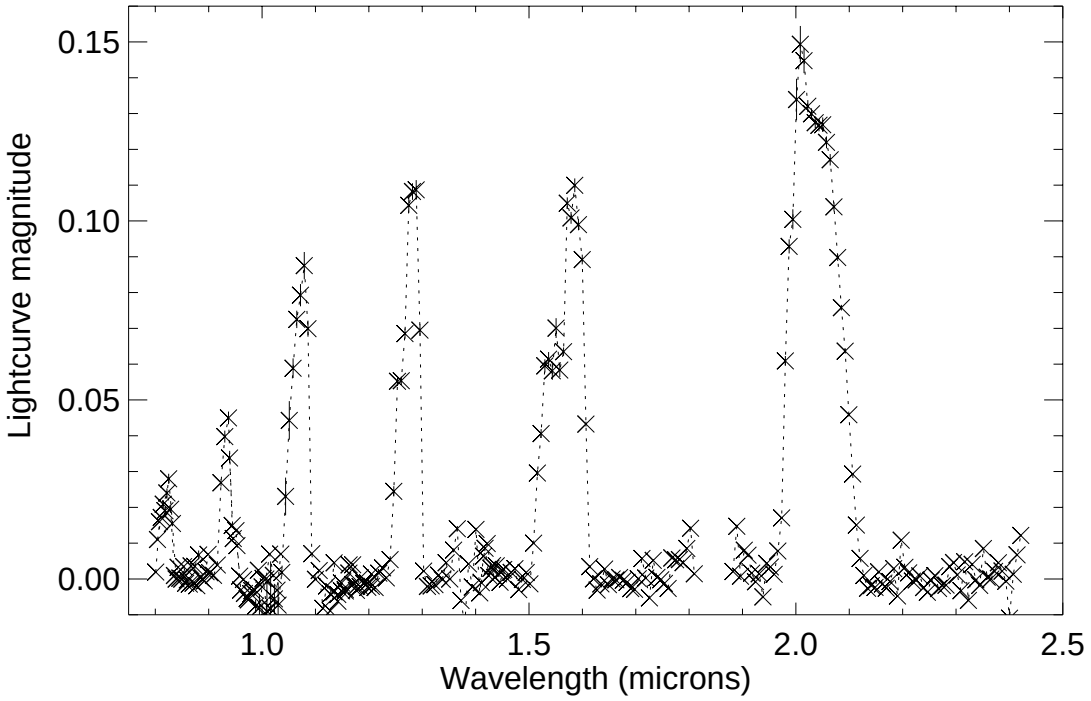

Figure 4.4 Fractional magnitude of Titan's lightcurve measured in 0.0075 micron wavelength bins. The six surface window regions are clearly visible. Titan's lightcurve is strongest at 2 microns with a magnitude of $\sim$15%.

4.4.2 Clouds

We can directly compare the amount of cloud activity in this dataset with that seen in a similar dataset from the 1990's (Griffith et al. 1998 and 2000). Cloud activity was inferred by Griffith et al. (1998) and (2000) by the presence of variability at 2.13-2.17 microns (which was also correlated with variability at 1.62-1.63 microns) on the wings of the 2.0 and 1.6 micron surface penetrating bands. Small variations at this wavelength range (where photons penetrate to the troposphere) corresponded to cloud activity of 0-0.8% at altitudes of approximately 30 km. When they subtracted a spectrum with extremely low cloud activity from all of the other observations, Griffith et al. (2000) saw variability in their residual spectra from 2.13 to 2.15 microns of approximately 0.002 on a daily basis. This type of variability is easily detectable in our dataset, yet on most nights we did not observe it.

In Figure 4.5 we show residual spectra (the spectrum from 2006-Feb-23 was subtracted from the same six spectra taken at with different central longitudes) compared with residual spectra from Griffith et al. (2000). The 2006-Feb-23 spectrum was chosen as a cloud-free night to subtract from the others because we have overlapping Gemini coverage on that night showing that no clouds were present. In contrast to the Griffith et al. (2000) residual spectra, most of our spectra deviate from each other shortward of 2.13 microns indicating a lack of clouds in Titan's troposphere. The three nights of Griffith et al. (2000) observations shown in Figure 4.5 correspond to 0.3%, 0.5% and 0.7% cloud coverage of Titan's disk at 30 km altitude. We can convert the residual flux at 2.13 microns to a total cloud coverage by scaling from the observations of Griffith et al. (2000) and find that on most nights Titan's total cloud coverage was less than 0.15% of its disk (Figure 4.6). On only 13% of the nights was cloud activity greater than 0.15% with 2-sigma error bars less than 0.15%. A Kolmogorov-Smirnov test of the central longitudes of the nights with clouds compared with the central longitudes of the nights without clouds reveals that they are not statistically different, indicating that the clouds we have observed are not clustered in

longitude. We find a slight increasing trend of cloud activity with time over the past two years. Clouds were observed on sequential nights on two occasions but generally lasted less than one earth night.

In addition to examining the residual flux at 2.13 microns, we can examine our lightcurves at slightly shorter (2.11-2.12 micron) wavelengths to search for clouds that may be lower in altitude (Figure 4.7). At 2.115 microns, Titan's surface lightcurve is just barely visible with an amplitude of less than 2%. Using a radiative transfer model (Toon et al., 1989; McKay et al., 1989; Ádámkovics et al., 2007) and assuming no cloud activity, we can construct a model of the expected lightcurve at this wavelength using the Cassini VIMS surface map (Barnes et al., 2007) as a base for the surface inputs. We find that there are 14 nights where the observed flux at 2.115 microns is 2-sigma above the modeled lightcurve. These nights all correspond to nights that we observed 2.13 micron residuals above 0.0005 (corresponding to cloud coverage of >0.15% microns at 30 km altitude) (Figures 4.5, 4.6, 4.7). Interestingly, on not all the nights we observed increased flux at 2.13 microns do we observe increased flux above the lightcurve at 2.115 microns. These are nights with central longitudes above the Xanadu feature. Clouds above the Xanadu feature are masked by its brightness and can only be observed at wavelengths longer than 2.13 microns where photons from the surface cannot penetrate.

4.4.3 Search for CO_2 Ice

The presence of CO_2 ice on the surface of Titan is expected due to possible volcanic outgassing from the interior. Adding all 138 spectra together (for a total integration time of ∼7 hours) we can search for the presence of the 2.012 and 2.070 micron CO_2 absorption features similarly to Hartung et al. (2006). We find no evidence for either of these two features. Using the absorption coefficients of 178 cm^{-1} and 31 cm^{-1} for the 2.012 and 2.070 micron features respectively from Quirico & Schmitt (1997) and assuming a linear mixture of water-ice and CO_2 we can constrain the amount of CO_2

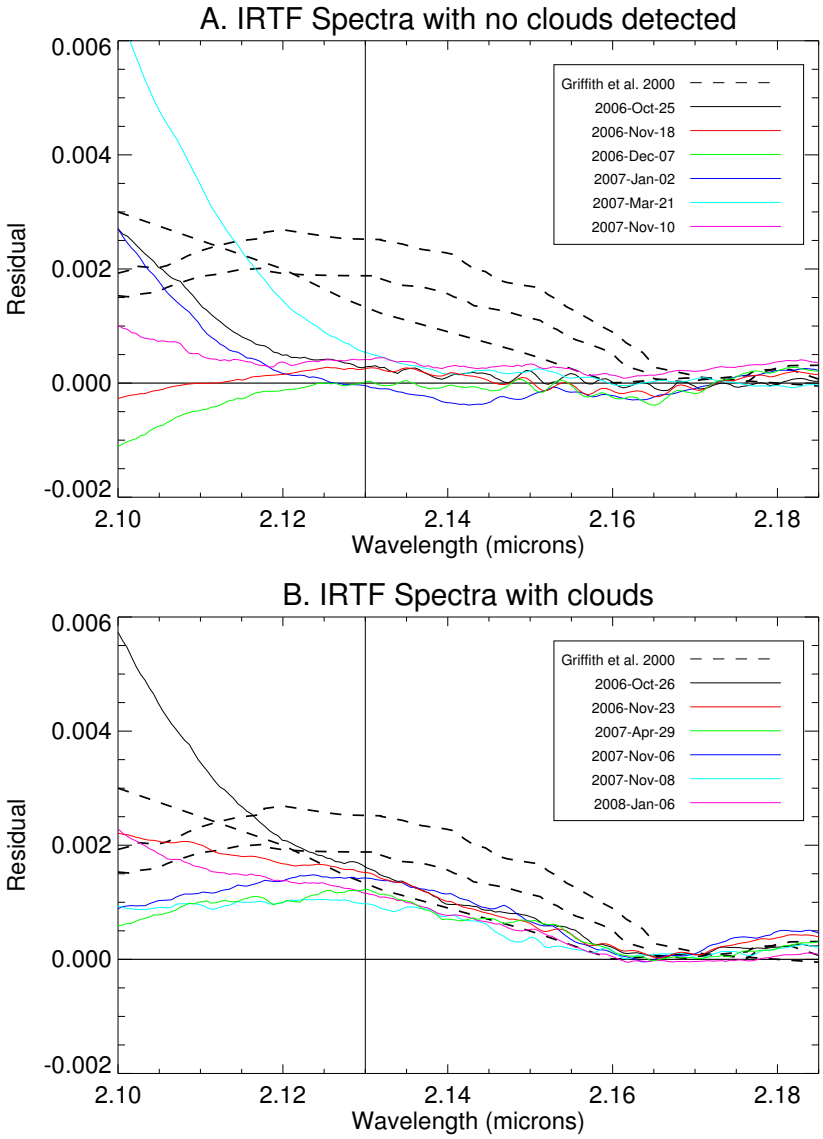

Figure 4.5 A. Titan residual spectra showing no evidence for tropospheric cloud activity. We subtracted a known night of no cloud activity (2006-Feb-23) from all other nights and examine the residual spectra. Longward of 2.17 microns, the spectra all lie on top of each other. The wavelengths at the locations of their deviations tell us about the presence and altitudes of tropospheric clouds. In the absence of clouds, all the spectra will deviate shortward of 2.13 μm (as do 87% of our IRTF spectra). Also shown are typical clouds observed by Griffith et al. (2000) from 1993-1999. These clouds covered 0.3%, 0.5% and 0.7% of Titan's surface respectively at altitudes of 30 km. B. IRTF spectra with clouds. Similarly to the Griffith et al. (2000) spectra, these spectra deviate at $\sim$2.16 microns. However, cloud activity in our observations was much less frequent (only 13% of nights) and generally covered less of Titan's disk than the Griffith et al. (2000) observations.

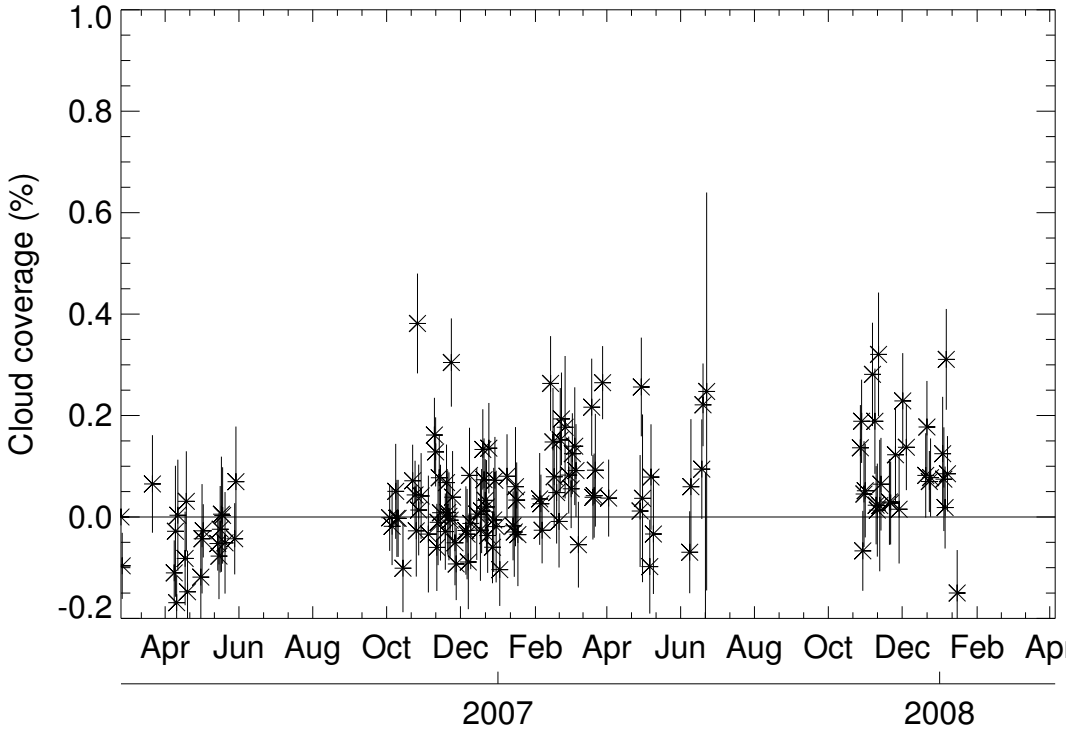

Figure 4.6 Titan residual flux at 2.13 microns allows us to determine the total fraction of Titan's disk that is covered by clouds (see also Figure 4.5). We find that on most nights Titan's clouds covered less than 0.15% of its disk in contrast with the Griffith et al. (2000) observations where cloud activity was detected in nearly all observations covering ∼0.5% of Titan's disk.

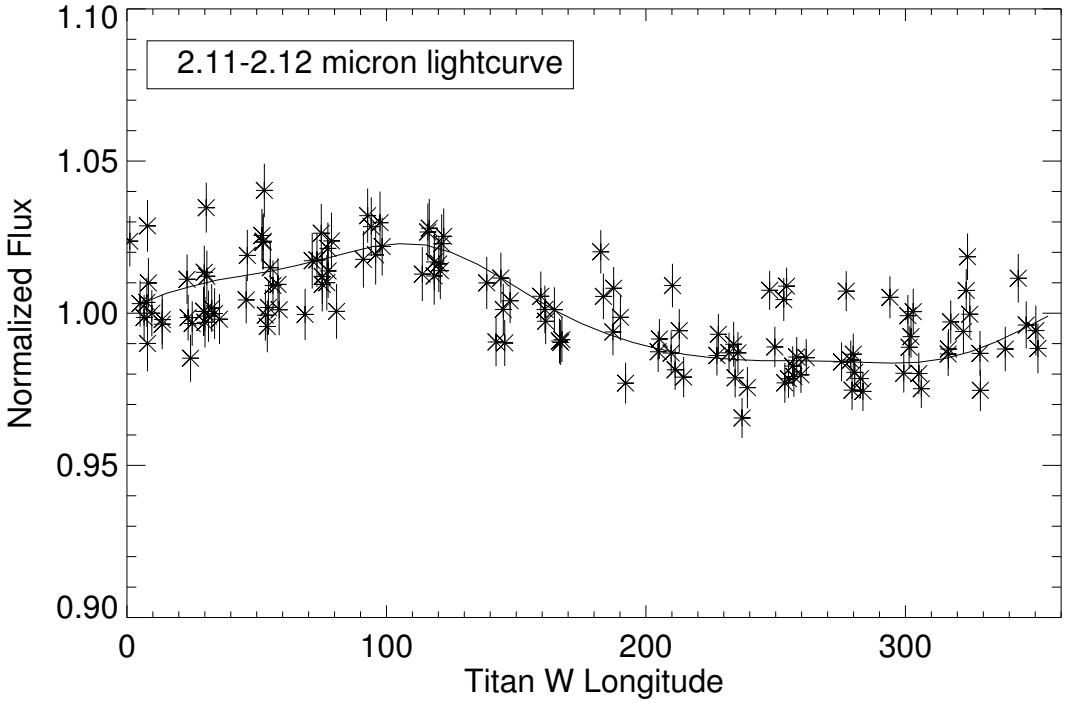

Figure 4.7 Titan's 2.11-2.12 micron lightcurve with a Titan radiative transfer model (Ádámkovics et al., 2007) assuming no tropospheric cloud activity (solid line). Nights on which Titan's flux is above the modeled surface lightcurve have cloud activity (these are the same nights that were observed to have cloud activity in the residual spectra).

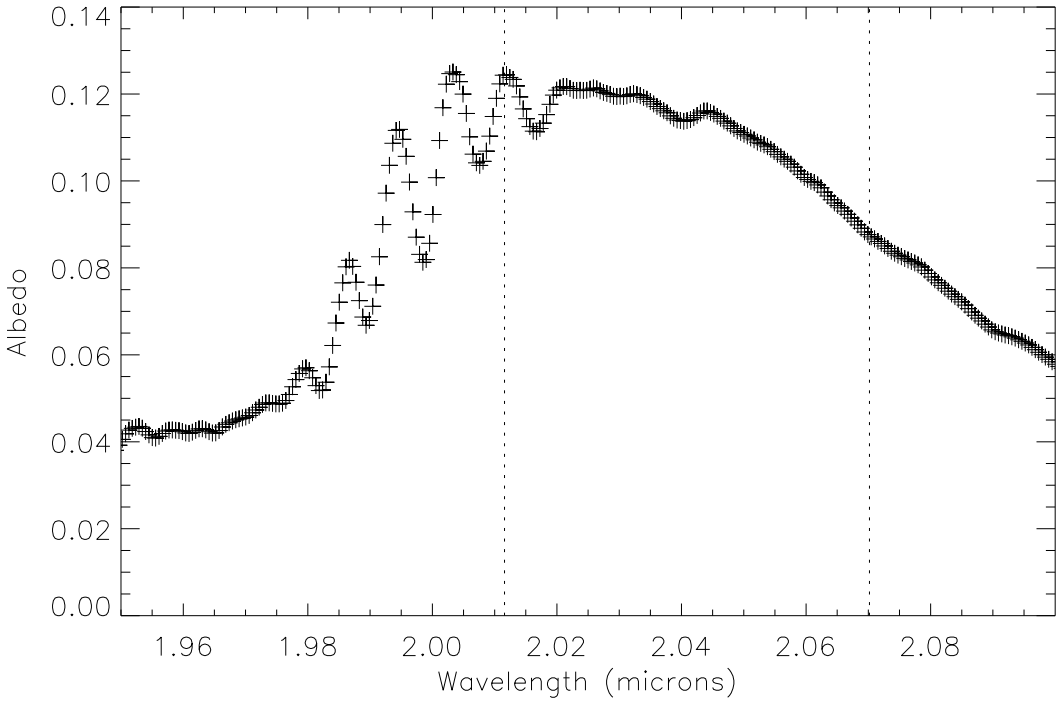

Figure 4.8 Spectra from all 138 nights of data are added together for a total integration time of ∼7 hours. Dotted lines show the expected positions of the narrow CO_2 ice absorption features (Quirico & Schmitt, 1997) that are not detected in our data

ice to be covering less than 5% of Titan's surface (assuming CO_2 grain sizes of 10 microns) (Figure 4.8). In addition, we added the spectra by phase to investigate the possibility that CO_2 may be concentrated in specific areas (it has been tentatively suggested CO_2 may be present in Tutti Regio) (McCord et al., 2008). We also found no evidence in any of the phase-added spectra for the presence of CO_2.

4.5 Discussion

The 138 nights of Titan IRTF observations span only 7% of a Titan year, the terrestrial equivalent of February 8 to March 6. Titan vernal equinox (i.e. March 21) will occur in August 2009. Our observations show that cloud activity on Titan has

markedly decreased in the pre-vernal equinox era compared with the southern summer solstice era (October 2002) (Brown et al., 2002; Roe et al., 2002; Bouchez & Brown, 2005; Schaller et al., 2006b) and the autumnal equinox era (1995) (Griffith et al., 1998, 2000). Unlike the Earth, where total cloud activity integrated over the whole surface only changes by several percent over the course of a year (from 58%-62% with northern hemisphere winter being cloudiest) (Thornes, 2002; Svensmark & Friis-Christensen, 1997), Titan's disk integrated cloud activity appears to undergo large-scale variations with season and with time (from essentially 0% to over 8%). The month of "February" on Titan appears to be extremely quiescent with only a small amount (covering less than 0.4% of Titan's disk at 30 km) of cloud activity occurring on less than 13% of the nights. Occasional Gemini images taken during this period confirm the decrease in cloud activity observed in the IRTF data (Roe et al. 2008 in prep). In addition, the few nights with cloud activity did not preferentially occur at a specific central longitude of observation, indicating that they may not be formed by the same mechanism or be related to the midlatitude clouds.

Though Titan's cloud activity has been rather quiescent of late, we expect that it will eventually resume. Several groups (Tokano, 2005; Rannou et al., 2006; Mitchell et al., 2006) have modeled Titan cloud locations with season using General Circulation Models (GCMs). These models make very different predictions regarding when and where Titan's clouds will resume. Though they all predict a decrease in cloud activity during the present season, the timing and locations of the resurgence are quite different. Rannou et al. (2006) predicts that south polar cloud activity should decrease but also predicts that cloud activity should be occurring near and 40 N which has never been observed. Rannou also predicts that clouds should begin forming over the north-pole and should be observed as soon as the north-pole comes into view. Tokano (2005) predicts the locations of superadiabatic zones and finds that these should only occur at the poles near the solstices, therefore predicting practically no cloud activity until 2014. Mitchell et al. (2006, 2007) predicts that clouds should slowly move toward

the equator near equinox (essentially following the area of maximum solar insolation with a slight phase lag) with decreased flux until the winter solstice when clouds will resume with full force near the north pole. The differences in these models are due to the uncertainties regarding the nature of Titan's surface (its thermal inertia) and other factors such as methane opacity, and haze and aeorsol distributions. Saturn's eccentric orbit around the sun also means that the insolation received at northern summer on Titan is approximately 10% less than that received at southern summer. This fact may lead to differences in southern and northern summer cloud activity. Indeed, the paucity of lakes seen by Cassini Radar in the south pole (Lunine et al., 2008) compared to the abundance in the north pole may be related to this insolation effect.

While infrequent observations from large telescopes and Cassini flybys are useful for studying the morphologies of clouds and occasional cloud outbursts, only a long-term near-nightly monitoring project has provided the type of dataset necessary to determine the frequency, duration, and altitudes of Titan's large clouds and daily cloud systems. Especially in this era of decreased cloud activity, near-nightly monitoring is also crucial for catching short-lived events and can provide context for Cassini flybys. Continued observations of Titan's clouds over the coming years will be critical for understanding the nature of Titan's hydrological cycle.

4.6 Conclusions

We have observed a seasonal change in the frequencies and brightenesses of Titan's tropospheric clouds. We observed cloud activity on only 13% of nights covering between 0.15% and 0.4% of Titan's disk at altitudes of ∼30 km. The frequencies and brightnesses of Titan's clouds have markedly decreased in the pre-vernal equinox era (2006-2008) compared with the time surrounding summer solstice (2001-2005) and autumnal equinox (1995-1999) indicating a seasonal change consistent with general

circulation models of Titan. This dataset provides a unique method for determining the amount of light from the surface that penetrates at a given wavelength — a useful metric for constraining radiative transfer models of Titan's atmosphere. We can also constrain the presence of CO_2 ice on Titan's surface to be less than 5% of the total observable area based on the lack of detection of the 2.012 micron and 2.07 micron CO_2 absorption features.

Acknowledgments: E.L.S. is supported by a NASA Graduate Student Research Fellowship. The data for this program were taken with the Infrared Telescope Facility, which is operated by the University of Hawaii under Cooperative Agreement no. NNX08AE38A with the National Aeronautics and Space Administration, Science Mission Directorate, Planetary Astronomy Program. This program would not have been possible without the nightly support of telescope operators Dave Greip, Bill Golish, Paul Sears, and Eric Volquardsen, who took most of the observations as service observing. We are grateful to Alan Tokunaga for initially believing in the program, to John Rayner and Bobby Bus for their assistance, and to all IRTF observers whose telescope time was interrupted by our program.

Table 4.1. IRTF Titan Observations

UT Date and Time	Ra and Dec	Airmass	Subsolar Long.	Clouds[a]
2006-02-23 07:31:08	08:33:00.78 19:30:56.8	1.0396000	282.690	
2006-02-24 07:27:13	08:32:47.37 19:31:43.8	1.0395000	305.160	
2006-03-21 06:28:04	08:28:11.55 19:51:55.0	1.0053333	147.650	
2006-04-08 05:12:15	08:27:09.89 19:55:07.5	1.0082000	192.160	
2006-04-09 04:58:36	08:27:06.37 19:54:58.9	1.0049167	214.540	
2006-04-10 04:53:17	08:27:05.61 19:54:18.0	1.0125000	237.020	
2006-04-11 05:04:47	08:27:06.48 19:53:45.1	1.0051667	259.730	
2006-04-17 05:55:42	08:27:54.96 19:52:03.2	1.0206667	35.6800	
2006-04-18 05:54:35	08:28:02.10 19:52:22.3	1.0230000	58.1900	
2006-04-19 05:57:44	08:28:09.00 19:52:29.4	1.0300000	80.7700	
2006-04-30 06:03:35	08:29:25.60 19:45:21.0	1.1043333	328.870	
2006-05-01 04:50:52	08:29:39.38 19:45:08.4	1.0120000	350.240	
2006-05-02 05:42:24	08:29:56.81 19:44:38.7	1.0775000	13.5800	
2006-05-14 05:10:39	08:32:27.71 19:34:50.0	1.1025000	283.610	
2006-05-15 05:08:22	08:32:46.93 19:33:51.6	1.1055000	306.110	
2006-05-16 05:14:21	08:33:08.39 19:32:45.8	1.1270000	328.720	
2006-05-17 05:01:22	08:33:29.67 19:31:52.5	1.1077500	351.040	
2006-05-18 05:04:23	08:33:51.79 19:31:00.4	1.1223750	13.6100	
2006-05-20 05:05:41	08:34:34.46 19:29:32.5	1.1432500	58.6700	
2006-05-28 05:05:41	08:36:47.09 19:20:14.8	1.2313333	239.080	
2006-05-29 05:15:45	08:37:07.50 19:18:34.2	1.2848333	261.780	
2006-10-03 14:49:44	09:36:42.31 15:11:24.7	2.0821667	253.530	
2006-10-05 15:36:37	09:37:30.88 15:07:21.4	1.5136667	299.350	
2006-10-08 15:15:17	09:38:49.62 15:02:17.0	1.5966667	6.60000	
2006-10-09 15:46:20	09:39:16.48 15:00:43.0	1.3693333	29.6100	
2006-10-14 15:40:25	09:41:02.50 14:53:55.4	1.3070000	142.230	
2006-10-22 15:21:24	09:43:21.20 14:41:05.8	1.2683333	322.340	
2006-10-24 15:39:24	09:44:06.25 14:38:33.9	1.1798333	7.67000	
2006-10-25 15:30:46	09:44:27.98 14:37:28.6	1.1955000	30.0600	
2006-10-26 15:53:49	09:44:48.48 14:36:29.1	1.1221667	52.9500	0.38%
2006-10-27 15:40:34	09:45:06.87 14:35:35.5	1.1461667	75.2800	
2006-10-29 15:27:16	09:45:37.30 14:33:48.2	1.1623333	120.170	
2006-11-04 14:48:20	09:46:41.12 14:26:57.2	1.2138333	254.930	
2006-11-09 15:31:12	09:47:56.90 14:22:01.5	1.0658333	8.26000	0.16%
2006-11-10 15:32:49	09:48:13.08 14:21:35.6	1.0578333	30.8000	

Table 4.1 (cont'd)

UT Date and Time	Ra and Dec	Airmass	Subsolar Long.	Clouds[a]
2006-11-11 15:33:27	09:48:27.72 14:21:02.8	1.0516667	53.3400	
2006-11-12 14:54:37	09:48:41.14 14:21:05.5	1.1141667	75.2700	
2006-11-13 15:29:39	09:48:50.32 14:20:16.9	1.0466667	98.3600	
2006-11-14 15:20:42	09:48:59.22 14:19:56.9	1.0538333	120.770	
2006-11-18 15:33:22	09:49:16.74 14:17:39.9	1.0230000	211.230	
2006-11-19 15:33:11	09:49:20.48 14:16:58.2	1.0201667	233.790	
2006-11-20 15:47:51	09:49:25.42 14:16:12.9	1.0095000	256.560	
2006-11-21 15:35:43	09:49:31.11 14:15:40.3	1.0135000	278.920	
2006-11-22 15:33:36	09:49:38.44 14:15:01.0	1.0126667	301.420	
2006-11-23 15:32:57	09:49:48.35 14:14:44.1	1.0110000	323.930	0.30%
2006-11-24 15:37:15	09:49:57.26 14:15:49.4	1.0076667	346.540	
2006-11-26 15:26:31	09:50:17.84 14:14:18.2	1.0090000	31.4200	
2006-11-27 15:34:08	09:50:25.47 14:14:29.1	1.0058333	54.0700	
2006-12-05 15:24:42	09:50:22.93 14:14:58.7	1.0061667	234.360	
2006-12-06 15:30:52	09:50:20.90 14:14:53.5	1.0091667	257.010	
2006-12-07 15:22:59	09:50:21.18 14:14:52.3	1.0076667	279.420	
2006-12-08 15:32:06	09:50:21.49 14:14:55.5	1.0135000	302.120	
2006-12-09 15:42:44	09:50:23.55 14:15:19.1	1.0233333	324.800	
2006-12-14 15:41:38	09:50:33.29 14:18:04.8	1.0418333	77.4300	
2006-12-17 15:37:34	09:50:16.50 14:20:28.8	1.0523333	145.020	
2006-12-18 15:38:43	09:50:06.43 14:21:02.8	1.0596667	167.600	
2006-12-19 15:39:36	09:49:55.69 14:21:40.9	1.0673333	190.180	
2006-12-20 15:44:54	09:49:44.07 14:22:14.2	1.0835000	212.830	
2006-12-21 15:49:21	09:49:34.06 14:22:40.5	1.1001667	235.460	
2006-12-22 15:53:04	09:49:25.46 14:23:11.3	1.1166667	258.080	
2006-12-23 15:42:39	09:49:18.26 14:23:46.9	1.1028333	280.450	
2006-12-24 15:43:22	09:49:13.14 14:24:21.3	1.1130000	303.000	
2006-12-27 14:39:10	09:49:01.91 14:27:01.9	1.0308333	9.58000	
2006-12-28 15:15:23	09:48:57.46 14:28:16.9	1.0881667	32.6600	
2006-12-29 15:19:53	09:48:51.72 14:29:35.2	1.1053333	55.2600	
2006-12-30 15:01:36	09:48:44.78 14:30:36.7	1.0781667	77.5100	
2007-01-02 15:27:09	09:48:06.69 14:35:03.7	1.1633333	145.570	
2007-01-08 14:21:01	09:46:33.80 14:40:59.8	1.0721667	279.880	
2007-01-13 15:40:34	09:45:44.95 14:47:55.0	1.4045000	33.7600	
2007-01-14 15:39:56	09:45:33.90 14:49:39.1	1.4245000	56.2700	

Table 4.1 (cont'd)

UT Date and Time	Ra and Dec	Airmass	Subsolar Long.	Clouds[a]
2007-01-15 15:40:31	09:45:20.87 14:51:25.8	1.4533333	78.8300	
2007-01-16 09:47:11	09:45:10.55 14:52:41.0	1.2591667	95.8400	
2007-01-17 09:47:54	09:44:53.22 14:54:25.6	1.2400000	118.390	
2007-02-04 10:21:59	09:39:27.78 15:23:46.6	1.0173333	164.740	
2007-02-05 10:19:54	09:39:03.15 15:25:18.9	1.0156667	187.270	
2007-02-06 10:12:50	09:38:39.07 15:26:43.4	1.0175000	209.730	
2007-02-13 10:39:50	09:36:36.53 15:37:17.8	1.0050000	7.91000	0.26%
2007-02-15 10:11:40	09:36:07.34 15:41:09.3	1.0030000	52.5200	
2007-02-16 10:01:13	09:35:51.35 15:42:37.4	1.0035000	74.9000	
2007-02-18 11:24:07	09:35:09.00 15:47:00.7	1.0630000	121.290	
2007-02-20 12:10:54	09:34:21.56 15:50:27.6	1.1901667	167.130	
2007-02-21 09:53:48	09:33:59.87 15:51:33.2	1.0028333	187.550	0.15%
2007-02-22 10:00:55	09:33:35.87 15:52:58.4	1.0045000	210.220	0.19%
2007-02-25 09:16:46	09:32:35.20 15:56:40.0	1.0045000	277.180	0.17%
2007-02-28 07:54:19	09:31:54.53 16:00:37.4	1.0698333	343.480	
2007-03-02 09:15:37	09:31:29.05 16:03:54.7	1.0020000	29.8000	
2007-03-03 09:19:56	09:31:16.62 16:05:38.5	1.0035000	52.3900	
2007-03-06 11:30:16	09:30:24.20 16:10:47.2	1.2538333	122.060	
2007-03-07 10:57:29	09:30:04.86 16:12:10.5	1.1590000	144.100	
2007-03-08 10:58:04	09:29:43.14 16:13:26.2	1.1731667	166.680	
2007-03-19 08:13:08	09:27:18.15 16:24:50.9	1.0031667	52.0200	0.22%
2007-03-20 04:51:58	09:27:07.44 16:26:04.2	1.3910000	71.4000	
2007-03-21 05:05:54	09:26:55.04 16:27:23.0	1.3006667	94.1600	
2007-03-22 04:52:20	09:26:43.59 16:28:23.9	1.3458333	116.500	
2007-03-28 07:22:47	09:25:13.31 16:32:20.7	1.0020000	254.190	0.26%
2007-04-02 05:28:2.	09:24:49.09 16:34:49.6	1.0895000	5.06000	
2007-04-28 06:21:05	09:23:41.10 16:38:30.8	1.0346667	232.010	
2007-04-29 04:49:43	09:23:43.30 16:37:52.0	1.0076667	253.120	0.26%
2007-04-30 04:31:28	09:23:47.99 16:37:06.7	1.0163333	275.380	
2007-05-06 08:46:35	09:24:46.33 16:34:30.5	1.7996667	54.5200	
2007-05-07 04:42:26	09:24:53.35 16:34:23.0	1.0020000	73.2400	
2007-05-09 04:50:37	09:25:06.39 16:33:35.6	1.0030000	118.450	
2007-06-08 07:19:22	09:31:57.66 15:58:46.8	2.3351667	77.0200	
2007-06-09 05:09:12	09:32:14.67 15:57:38.1	1.2201667	97.5200	
2007-06-18 05:38:44	09:34:56.68 15:41:17.2	1.5451667	300.940	

Table 4.1 (cont'd)

UT Date and Time	Ra and Dec	Airmass	Subsolar Long.	Clouds[a]
2007-06-19 05:35:52	09:35:22.39 15:39:38.4	1.5694167	323.420	0.22%
2007-06-21 05:05:23	09:36:14.11 15:36:05.2	1.3860000	7.91000	
2007-06-22 05:07:02	09:36:41.13 15:34:12.4	1.4270000	30.5600	
2007-10-27 15:15:21	10:33:22.72 10:37:44.8	1.4895000	23.1600	
2007-10-28 15:59:22	10:33:46.77 10:36:09.1	1.2473333	46.3800	0.19%
2007-10-29 15:41:05	10:34:08.58 10:34:38.1	1.3081667	68.6400	
2007-10-30 15:38:43	10:34:28.77 10:33:09.6	1.3026667	91.1300	
2007-10-31 15:46:25	10:34:47.07 10:31:38.0	1.2555000	113.810	
2007-11-06 14:08:12	10:36:10.38 10:22:04.9	1.7478333	247.650	0.28%
2007-11-08 15:30:53	10:36:44.75 10:19:00.6	1.2066667	294.020	0.19%
2007-11-09 15:31:42	10:37:03.69 10:17:27.9	1.1926667	316.570	
2007-11-10 14:50:07	10:37:22.84 10:16:15.5	1.3430000	338.460	
2007-11-11 14:58:21	10:37:42.66 10:15:02.4	1.2886667	1.11000	0.32%
2007-11-12 14:53:25	10:38:01.74 10:13:51.7	1.2943333	23.5600	
2007-11-13 14:44:24	10:38:20.77 10:12:45.4	1.3185000	45.9500	
2007-11-20 15:40:51	10:39:41.46 10:05:35.9	1.0776667	204.710	
2007-11-21 15:44:03	10:39:48.94 10:04:31.6	1.0670000	227.340	
2007-11-25 15:40:43	10:40:32.76 10:00:42.4	1.0515000	317.450	
2007-11-28 15:48:21	10:41:14.44 09:58:51.2	1.0326667	25.1600	
2007-12-01 15:46:33	10:41:47.66 09:57:34.6	1.0260000	92.7400	0.23%
2007-12-04 14:47:17	10:42:01.24 09:56:17.5	1.0798333	159.490	
2007-12-20 15:40:04	10:42:54.34 09:55:30.8	1.0250000	161.070	
2007-12-21 15:38:31	10:42:49.11 09:55:46.7	1.0266667	183.600	0.18%
2007-12-23 14:44:47	10:42:37.93 09:56:05.0	1.0161667	227.890	
2007-12-24 13:55:13	10:42:33.34 09:56:21.5	1.0445000	249.670	
2007-12-27 13:08:24	10:42:29.66 09:57:31.8	1.0995000	316.450	
2008-01-03 14:53:51	10:42:19.10 10:03:22.3	1.0323333	115.950	
2008-01-04 15:01:51	10:42:10.58 10:04:22.2	1.0435000	138.640	
2008-01-05 15:10:59	10:41:59.32 10:05:12.6	1.0595000	161.340	
2008-01-06 13:46:15	10:41:48.50 10:06:00.3	1.0161667	182.590	0.31%
2008-01-07 13:47:25	10:41:35.72 10:06:47.7	1.0150000	205.170	
2008-01-15 12:44:58	10:40:34.81 10:15:20.9	1.0266667	24.5100	

[a]Cloud coverage of Titan's disk. 2σ error bars are $\sim$0.15% on most nights (see Fig 4.6). Cloud activity is only listed if it is above 0.15% with an error bar less than 0.15%.

Bibliography

Ádámkovics, M., Wong, M. H., Laver, C., & de Pater, I. 2007, Science, 318, 962

Barnes, J. W., Brown, R. H., Soderblom, L., Buratti, B. J., Sotin, C., Rodriguez, S., Le Mouèlic, S., Baines, K. H., Clark, R., & Nicholson, P. 2007, Icarus, 186, 242

Bouchez, A. H. & Brown, M. E. 2005, Astrophysical Journal, Letters, 618, L53

Brown, M. E., Bouchez, A. H., & Griffith, C. A. 2002, Nature, 420, 795

Cushing, M. C., Vacca, W. D., & Rayner, J. T. 2004, Publications of the ASP, 116, 362

Griffith, C. A., Hall, J. L., & Geballe, T. R. 2000, Science, 290, 509

Griffith, C. A., Owen, T., Miller, G. A., & Geballe, T. 1998, Nature, 395, 575

Griffith, C. A., Penteado, P., Baines, K., Drossart, P., Barnes, J., Bellucci, G., Bibring, J., Brown, R., Buratti, B., Capaccioni, F., Cerroni, P., Clark, R., Combes, M., Coradini, A., Cruikshank, D., Formisano, V., Jaumann, R., Langevin, Y., Matson, D., McCord, T., Mennella, V., Nelson, R., Nicholson, P., Sicardy, B., Sotin, C., Soderblom, L. A., & Kursinski, R. 2005, Science, 310, 474

Hartung, M., Herbst, T. M., Dumas, C., & Coustenis, A. 2006, Journal of Geophysical Research (Planets), 111, 7

Lorenz, R. D., Mitchell, K. L., Kirk, R. L., Hayes, A. G., Aharonson, O., Zebker, H. A., Paillou, P., Radebaugh, J., Lunine, J. I., Janssen, M. A., Wall, S. D., Lopes, R. M., Stiles, B., Ostro, S., Mitri, G., & Stofan, E. R. 2008, Geophysics Research Letters, 35, 2206

Lunine, J. I., Mitri, G., Elachi, C., Stofan, E. R., Lorenz, R. D., Kirk, R. L., Michell, K., Lopes, R. M. C., Wood, C. A., Radebaugh, J., Wall, S. D., Soderblom, L. A.,

Pallou, P., Farr, T., Stiles, B., Callahan, P., & Cassini Radar Team. 2008, in Lunar and Planetary Inst. Technical Report, Vol. 39, Lunar and Planetary Institute Conference Abstracts, 1637–+

McCord, T. B., Hayne, P., Combe, J.-P., Hansen, G. B., Barnes, J. W., Rodriguez, S., Le Mouélic, S., Baines, E. K. H., Buratti, B. J., Sotin, C., Nicholson, P., Jaumann, R., Nelson, R., & The Cassini Vims Team. 2008, Icarus, 194, 212

McKay, C. P., Pollack, J. B., & Courtin, R. 1989, Icarus, 80, 23

Mitchell, J., Pierrehumbert, R. T., & Lorenz, R. D. 2007, in AAS/Division for Planetary Sciences Meeting Abstracts, Vol. 39, AAS/Division for Planetary Sciences Meeting Abstracts, 56.18–+

Mitchell, J. T., Pierrehumbert, R. T., Frierson, D. M., & Caballero, R. PNAS, 103, 18421.

Quirico, E. & Schmitt, B. 1997, Icarus, 127, 354

Rannou, P., Montmessin, F., Hourdin, F., & Lebonnois, S. 2006, Science, 311, 201

Rayner, J. T., Toomey, D. W., Onaka, P. M., Denault, A. J., Stahlberger, W. E., Vacca, W. D., Cushing, M. C., & Wang, S. 2003, Publications of the ASP, 115, 362

Roe, H. G., Bouchez, A. H., Trujillo, C. A., Schaller, E. L., & Brown, M. E. 2005a, Astrophysical Journal, Letters, 618, L49

Roe, H. G., Brown, M. E., Schaller, E. L., Bouchez, A. H., & Trujillo, C. A. 2005b, Science, 310, 477

Roe, H. G., de Pater, I., Macintosh, B. A., & McKay, C. P. 2002, Astrophysical Journal, 581, 1399

Schaller, E. L., Brown, M. E., Roe, H. G., & Bouchez, A. H. 2006a, Icarus, 182, 224

Schaller, E. L., Brown, M. E., Roe, H. G., Bouchez, A. H., & Trujillo, C. A. 2006b, Icarus, 184, 517

Soderblom, L. A., Tomasko, M. G., Archinal, B. A., Becker, T. L., Bushroe, M. W., Cook, D. A., Doose, L. R., Galuszka, D. M., Hare, T. M., Howington-Kraus, E., Karkoschka, E., Kirk, R. L., Lunine, J. I., McFarlane, E. A., Redding, B. L., Rizk,

B., Rosiek, M. R., See, C., & Smith, P. H. 2007, Planetary Space Science, 55, 2015

Stofan, E. R., Elachi, C., Lunine, J. I., Lorenz, R. D., Stiles, B., Mitchell, K. L., Ostro, S., Soderblom, L., Wood, C., Zebker, H., Wall, S., Janssen, M., Kirk, R., Lopes, R., Paganelli, F., Radebaugh, J., Wye, L., Anderson, Y., Allison, M., Boehmer, R., Callahan, P., Encrenaz, P., Flamini, E., Francescetti, G., Gim, Y., Hamilton, G., Hensley, S., Johnson, W. T. K., Kelleher, K., Muhleman, D., Paillou, P., Picardi, G., Posa, F., Roth, L., Seu, R., Shaffer, S., Vetrella, S., & West, R. 2007, Nature, 445, 61

Svensmark, H. & Friis-Christensen, E. 1997, Journal of Atmospheric and Terrestrial Physics, 59, 1225

Thornes, J. E. 2002, International Journal of Climatology, 22, 1285

Tokano, T. 2005, Icarus, 173, 222

Toon, O. B., McKay, C. P., Ackerman, T. P., & Santhanam, K. 1989, Journal of Geophysics Research, 94, 16287

Chapter 5

Volatile Loss and Retention on Kuiper Belt Objects

This chapter has been published in its entirety under the same title by authors E.L. Schaller and M.E. Brown in *Astrophysical Journal Letters*, 2007, Volume 659, pp. 61–64.

5.1 Abstract

Recent discoveries have shown that the very largest Kuiper belt objects – Eris, 2005 FY9 and Sedna – are coated in methane, and may contain other volatile ices as well. New detailed observations show that even within this class of volatile-rich bodies unexpected differences exist in their surface compositions. 2005 FY9, a body approximately 60% the size of Pluto, with a reflectance spectrum similarly dominated by methane, has a surface depleted in molecular nitrogen by at least an order in magnitude with respect to Pluto. We find that the existence this new class of volatile-rich objects, the lack of volatiles on most Kuiper belt objects, and even the otherwise peculiar surface of 2005 FY9 can be explained as a consequence of atmospheric escape of volatile compounds. While previous studies of the surface compositions of objects in the Kuiper belt have found no explainable patterns, atmospheric escape appears to provide a first-order explanation of the range of surface spectra seen on bodies in the outer solar system.

5.2 Introduction

Pluto and Neptune's satellite Triton have long been known to be covered in methane, molecular nitrogen and carbon monoxide ices that sublime and form the tenuous atmospheres seen surrounding these bodies (Cruikshank et al., 1976; Cruikshank & Silvaggio, 1979; Owen et al., 1993; Cruikshank et al., 1993). Until recently these volatile-rich surfaces appeared to be unique in the outer solar system. A decade of observations of small Kuiper belt objects (KBOs) found that these bodies were covered in involatile water-ice or had flat spectra with nothing identifiable (Luu & Jewitt, 1998; Brown et al., 1999; Jewitt & Luu, 2001; Grundy et al., 2005; Trujillo et al., 2005). The recent discoveries of methane on large KBOs Eris, Sedna, and 2005 FY9 have shown that these objects are part of a new class of volatile-rich bodies in the outer solar system (Brown et al., 2005; Licandro et al., 2006; Barucci et al., 2005;

Brown et al., 2007). Even among these objects, however, there are differences in the relative abundances of the three volatile ices (CH_4, N_2 and CO). For example the spectrum of large KBO 2005 FY9 is dominated by broad absorption features due to long path lengths through solid CH_4 with trace amounts of solid ethane also detected (Brown et al., 2007). The lack of detection of an N_2 absorption feature, the long path lengths of CH_4, and the detection of ethane were all interpreted as being due to a depletion of at least an order of magnitude of molecular nitrogen relative to methane on 2005 FY9 compared to Pluto (Brown et al., 2007).

To understand volatile loss and retention on Kuiper belt objects, we have constructed a simple model of atmospheric escape that allows us to predict which bodies should be capable of retaining which surface volatile ices to the present day. While it has long been expected that large and cold bodies in the outer solar system should have the potential of retaining their volatile ices (Stevenson, 1993), the recent proliferation of new discoveries in the Kuiper belt provides us with a range of bodies with varying sizes and orbits on which to test predictions of volatile loss and retention.

5.3 Atmospheric Escape

The materials from which the bodies in the outer solar system accreted were rich in volatile ices; small primordial bodies such as comets contain several percent fractions of methane, nitrogen, and carbon monoxide (Krankowsky et al., 1986; Eberhardt et al., 1987; Jessberger et al., 1989). When these volatile ices are accessible to the surface they will sublime and may form a vapor pressure controlled atmosphere. Depending on the mass and temperature of the body, atmospheric escape can occur through a variety of processes.

On Earth, light elements like hydrogen are lost through the thermal evaporation of particles in the high-velocity tail of the Maxwellian distribution through a process known as Jeans escape. On low mass Kuiper belt objects, the heavier volatile species

(CH_4, N_2 and CO) can be efficiently lost via this process. An even faster loss process that can occur on low mass or high temperature objects is hydrodynamic escape. This process occurs when the atmosphere flows away from the body at supersonic speeds such as occurs on comets. However, even on Pluto and Triton, where the thermal structures of the atmospheres are well known, it is difficult to calculate a priori from what regime (Jeans or hydrodyamic) escape is occurring. Additionally, in cases of bodies with eccentric orbits like Pluto, the escape regime may vary over the course of the orbit (Trafton et al., 1997).

Of the two processes, Jeans loss provides a lower limit to the escape flux, but even with Jeans loss the escape rate is a very sensitive function of the temperature and height of the exobase, the location from which the escape is occurring. EUV heating of the upper atmosphere can cause the exobase temperature to be greatly elevated over the surface radiative equilibrium temperature, significantly increasing the escape rate. Consequently the exobase temperature – and thus the true escape rate – cannot be calculated without a detailed knowledge of the thermal structure and composition of the atmosphere. While an accurate estimate of the true escape flux appears impossible, a reasonable lower bound to the escape rate can be found by simply assuming that the exobase is at the surface and by calculating the Jeans escape flux using the surface radiative equilibrium temperature. This calculated escape flux will be lower than any actual flux from any atmosphere where the exobase is elevated above the surface and has a temperature equal to or greater than the surface temperature. The only situations in which this lower bound fails is for an atmosphere with an exobase temperature lower than the surface temperature. All comparable planetary atmospheres suffer EUV heating in the upper atmosphere and have elevated temperatures, thus we deem this possibility remote, and consider the surface Jeans escape rate to be a reasonable lower bound when the details of individual KBO atmospheres are unknown.

We model the Jeans escape flux (Chamberlain & Hunten, 1987) of CH_4, N_2 and

CO from a body with radius R with a surface in radiative equilibrium as

$$\frac{dM_{vol}}{dt} = 4\pi R^2 \frac{P_{vap}(T)}{2\sqrt{\pi}kT}\sqrt{\frac{2kT}{m}}(1+\lambda)e^{-\lambda},$$

where

$$\lambda = \frac{GMm}{kTR}$$

$\frac{dM_{vol}}{dt}$ is the rate of loss of a given volatile in molecules per second, P_{vap}(T) is the vapor pressure of a given volatile compound (Lodders & Fegley, 1998) at T, the radiative equilibrium temperature, k is the Boltzmann constant, m is the molecular mass of a given volatile species, G is the gravitational constant and M is the mass of the body.

To explore volatile loss on bodies in the outer solar system, we calculated the minimum volatile loss a body of a given size and temperature could have experienced and compared it to the maximum initial volatile inventory it could have accessible to the surface. If a body is capable of losing its total inventory of volatiles through the slowest loss mechanism (Jeans escape assuming the surface radiative equilibrium temperature), examination of other loss processes (such as hydrodynamic escape, Jeans escape occurring from a higher temperature exobase, UV photolysis) is unnecessary as these processes will only deplete volatiles even faster. In addition, the mass of accessible volatile ices may be significantly less than the maximum initial inventory because volatiles may be locked away at depth and shielded from the surface, making depletion of surface volatiles occur even more rapidly. Therefore, for a body of a given size and surface temperature and assuming all volatiles are accessible to the surface, we calculate the total minimum volatile loss from Jeans escape over the age of the solar system.

In Figure 1 we show where this total minimum loss is equal to the approximate initial inventory of these volatiles for a given size and temperature assuming a density of 1.8 g/cm^3. We assumed initial volatile inventories equal to the maximum gas production rate relative to water released from the nucleus of Comet Halley for CH_4,

N_2 and CO (0.07, 0.02, and 0.07 respectively) (Jessberger et al., 1989) and scaled by the rock-water mass fraction of Charon (Gulbis et al., 2006). Note that changing these initial volatile abundances by an order of magnitude does not appreciably change the positions of the lines in Figure 1 as they are controlled mainly by the vapor pressures of the compounds. Small and hot objects will have lost all of their accessible volatiles due to Jeans escape, while large and cold objects will not have necessarily been depleted in these volatiles via this process. Objects between the extremes are capable of losing some volatile species while retaining others.

In order to model minimum volatile loss on the currently known Kuiper belt objects, we assume that all bodies began as volatile-rich, high-albedo objects similar to Pluto with all volatiles at the surface equilibrium temperature and accessible to the surface. For each of the known Kuiper belt objects, we numerically calculate the volatile loss by dividing the object's orbit into small segments and integrating the total loss volatile over the age of the solar system. Finally, we translate this total mass loss into a volatile loss equivalent temperature corresponding to the temperature of an identical mass body in a circular orbit that would have experienced the same loss over the age of the solar system. The equivalent volatile loss temperature for most bodies is very close to the perihelion temperature since most of the loss occurs near perihelion. However, for objects with extremely eccentric orbits the equivalent temperature can be somewhat lower.

5.4 Results and Discussion

The known Kuiper belt objects divide into three general categories in this analysis (Figure 1). (1) The large majority are too small and too hot to have retained any surface volatiles even with this minimum escape mechanism. (2) A small number of the largest objects have such low escape fluxes that even escape mechanisms many orders of magnitudes more effective will not be able to deplete their volatiles. (3)

Three objects (2003 EL61, Quaoar and 2005 FY9) exist near the transition between possible volatile retention and certain volatile loss.

The first two categories predicted by the atmospheric escape model perfectly reflect known KBO surface compositions. No KBOs which are predicted to be too small and hot to preserve volatiles have had volatiles detected on their surfaces, while all of the KBOs which are predicted to be large and cold enough to easily maintain volatiles indeed have had volatiles detected (Table 1). If volatiles were to be detected on the surface of any of the small hot bodies, their unexpected presence would have to be explained by a recent impact or other transient event that liberated stored volatiles from the subsurface or by a geochemical mechanism such as serpentinization that produced volatiles in the interior of the body.

The most interesting behavior occurs for the three objects near the line between certain loss and possible volatile retention. The transition region is also the location where different volatiles will be lost at different rates. For the lower mass or higher temperature bodies, vapor pressure dominates over gravitational attraction, so the volatile species with higher vapor pressures, like N_2 and CO, will escape the fastest. On the higher mass or lower temperature bodies, in contrast, gravitational attraction is dominant and lower molecular weight species, like methane, will escape the fastest.

The first transition object, 2003 EL61, is one of the most unusual bodies in the solar system. This rapidly spinning 2000 x 1500 x 1000 km body (Rabinowitz et al., 2006) has a spectrum dominated by water ice and has no evidence for the presence of any volatile ices (Trujillo et al., 2007). However, the high density, fast rotation rate, and multiple satellite system of 2003 EL61 (Brown et al., 2006b) suggest that it experienced a disruptive collision where it lost most of its water ice and likely all of its volatiles as well.

Quaoar is also in the transition region between complete volatile loss and possible volatile retention. This object has a water-ice dominated spectrum with an additional absorption feature at 2.2-microns that has not been seen on any other smaller KBOs.

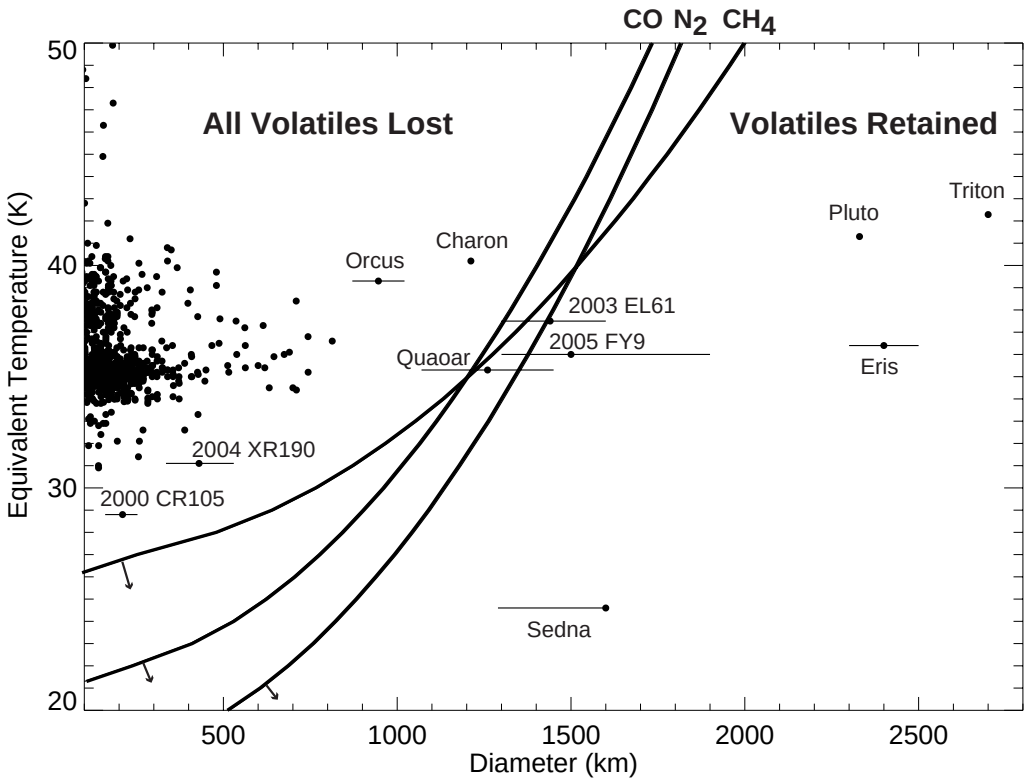

Figure 5.1 Minimum volatile loss in the outer solar system as a function of temperature and radius. The lines show the temperatures as a function of radius at which the initial inventories of CH_4, N_2 and CO must be lost over the age of the solar system. Note that changing these initial volatile abundances by an order of magnitude does not appreciably change the positions of the lines as they are controlled mainly by the vapor pressures of the compounds. The arrows show the distance each line would congruently shift if we assumed only 10% of the initial volatile inventory is accessible to the surface. The known KBOs are plotted on this figure by considering their equivalent volatile loss temperatures. To find this temperature we calculate the loss of N_2, CH_4, and CO at each position in the object's orbit and integrate the total loss over the age of the solar system. We then translate this total mass loss into a temperature corresponding to the temperature of an identical body in a circular orbit that would have experienced the same loss over the age of the solar system. For KBOs with unknown sizes, we assumed an albedo of 0.1 to calculate the size.

The feature has been interpreted as an absorption due to non-volatile ammonia ices (Jewitt & Luu, 2004), but it has also been argued to be due to trace amounts of methane on the surface (Brown, 2003), consistent with Quaoar being an object that may still retain some initial volatiles. Higher quality spectra to explore the surface of this object are clearly warranted.

The final transition object is the methane-rich but nitrogen depleted 2005 FY9. 2005 FY9 exists near the region where N_2 must be depleted but CH_4 and CO can possibly remain. The formerly unexplained depletion of nitrogen seen in the spectrum of this object may be explained by differential atmospheric loss of N_2 relative to CH_4. The presence of volatiles on 2005 FY9 appears to rule out hydrodyamic escape occuring over the age of the solar system on this body. The minimum hydrodynamic escape rate is nearly 2 orders of magnitude greater than the Jeans escape rate for a body of this size and temperature.

Atmospheric loss appears to explain not only the presence and absence of volatiles, but may also be able to explain the balance of the individual volatile ices present bodies of the outer solar system. More detailed modeling would be required to predict more accurate escape rates, but such modeling does not appear necessary for an initial description of the range of spectra presently seen on bodies in the outer solar system. While it is perhaps surprising that the simple lower bound escape rate seems to accurately predict loss on the transition objects, it may be that initial loss rates are higher but that this mechanism is the rate limiting step when objects are close to depleting all of their volatiles. Objects could thus spend significant time periods near this transition region. As more objects are discovered in the Kuiper belt with high perihelia orbits similar to Sedna's, we expect that all but the smallest of these objects could contain volatile ices on their surfaces and may show depletions in nitrogen similar to 2005 FY9.

Acknowledgments: We thank John Stansberry for a helpful review and David Stevenson, Kristina Barkume, Henry Roe, Oded Aharonson and Re'em Sari for helpful

discussions.

Table 5.1 Sizes, orbits and surface characteristics of objects in Figure 5.1

Body	Diameter (km)	ref	Perihelion (AU)	Aphelion (AU)	Known surface volatiles	ref
Eris	2400 ±100	1	37.8	97.6	CH_4, N_2	2,3
Pluto	2328 ±46	4	29.7	49.3	CH_4, N_2, CO	5,6
Charon	1212 ±16	7	29.7	49.3	None	8
Triton	2700	9	29.8	30.3	CH_4, N_2, CO	10,11
2003 EL61	2000x1500x1000	12	35.1	51.5	None	13
Sedna	< 1600 [a]		76.2	975.1	CH_4, N_2?	14
2005 FY9	1500 ±300 [a]		38.5	53.1	CH_4	15,16
Quaoar	1260 ±190	17	41.9	44.9	None, CH_4?	18,19
Orcus	950 ±70 [a]		30.5	48.3	None	20,21
2004 XR190	335-530 [b]		52.3	61.8	Unknown	
2000 CR105	160-253 [b]		44.4	397.6	Unknown	

[a] Diameters from Stansberry, J.A. et al. Thermal Detection of KBOs: Albedos sizes and densities, to appear in Kuiper Belt (eds Barucci, M.A., Boehnhardt, H., Cruikshank, D., Morbedelli, A.)

[b] Diameter range estimated by assuming 10-25% albedo

References. — (1)(Brown et al., 2006a); (2)(Brown et al., 2005); (3)(Licandro et al., 2006b); (4)(Young & Binzel, 1993); (5)(Cruikshank et al., 1976); (6)(Owen et al., 1993); (7)(Gulbis et al., 2006); (8)(Brown & Calvin, 2000); (9)(Smith et al., 1989); (10)(Cruikshank & Silvaggio, 1979); (11)(Cruikshank et al., 1993); (12)(Rabinowitz et al., 2006); (13)(Trujillo et al., 2007); (14)(Barucci et al., 2005); (15)(Licandro et al., 2006); (16)(Brown et al., 2007); (17)(Brown & Trujillo, 2004); (18)(Jewitt & Luu, 2004); (19)(Brown, 2003); (20)(de Bergh et al., 2005); (21)(Trujillo et al., 2005)

Bibliography

Barucci, M. A., Cruikshank, D. P., Dotto, E., Merlin, F., Poulet, F., Dalle Ore, C., Fornasier, S., & de Bergh, C. 2005, Astronomy and Astrophysics, 439, L1

Brown, M. E. 2003, AAS/DPS Meeting, 35, 29.01

Brown, M. E., Barkume, K. M., Blake, G. A., Schaller, E. L., Rabinowitz, D. L., Roe, H. G., & Trujillo, C. A. 2007, Astronomical Journal, 133, 284

Brown, M. E. & Calvin, W. M. 2000, Science, 287, 107

Brown, M. E., Schaller, E. L., Roe, H. G., Rabinowitz, D. L., & Trujillo, C. A. 2006a, Astrophysical Journal, Letters, 643, L61

Brown, M. E. & Trujillo, C. A. 2004, Astronomical Journal, 127, 2413

Brown, M. E., Trujillo, C. A., & Rabinowitz, D. L. 2005, Astrophysical Journal, Letters, 635, L97

Brown, M. E., et al. 2006b, Astrophysical Journal, Letters, 639, L43

Brown, R. H., Cruikshank, D. P., & Pendleton, Y. 1999, Astrophysical Journal, Letters, 519, L101

Chamberlain, J. W. & Hunten, D. M. 1989, Theory of Planetary Atmospheres, (2d ed.; San Diego: Academic Press Inc.)

Cruikshank, D. P., Pilcher, C. B., & Morrison, D. 1976, Science, 194, 835

Cruikshank, D. P., Roush, T. L., Owen, T. C., Geballe, T. R., de Bergh, C., Schmitt, B., Brown, R. H., & Bartholomew, M. J. 1993, Science, 261, 742

Cruikshank, D. P. & Silvaggio, P. M. 1979, Astrophysical Journal, 233, 1016

de Bergh, C., Delsanti, A., Tozzi, G. P., Dotto, E., Doressoundiram, A., & Barucci, M. A. 2005, Astronomy and Astrophysics, 437, 1115

Eberhardt, P., et al. 1987, Astronomy and Astrophysics, 187, 481

Grundy, W. M., Buie, M. W., & Spencer, J. R. 2005, Astronomical Journal, 130, 1299

Gulbis, A. A. S., et al. 2006, Nature, 439, 48

Jessberger, E. K., Kissel, J., & Rahe, J. in Origin and Evolution of Planetary and Satellite Atmospheres, ed. S.K. Atreya, J.B Pollack, M.S. Matthews (Tuscon: University of Arizona Press), 167

Jewitt, D. C. & Luu, J. 2004, Nature, 432, 731

Jewitt, D. C. & Luu, J. X. 2001, Astronomical Journal, 122, 2099

Krankowsky, D., et al. 1986, Nature, 321, 326

Licandro, J., Pinilla-Alonso, N., Pedani, M., Oliva, E., Tozzi, G. P., & Grundy, W. M. 2006b, Astronomy and Astrophysics, 445, L35

Licandro, J., Grundy, W. M., Pinilla-Alonso, N., & Leisy, P. 2006a, Astronomy and Astrophysics, 458, L5

Lodders, K. & Fegley, B. 1998, The planetary scientist's companion (New York: Oxford University Press)

Luu, J. X. & Jewitt, D. C. 1998, Astrophysical Journal, Letters, 494, L117

Owen, T. C., et al. 1993, Science, 261, 745

Rabinowitz, D. L., Barkume, K., Brown, M. E., Roe, H., Schwartz, M., Tourtellotte, S., & Trujillo, C. 2006, Astrophysical Journal, 639, 1238

Smith, B. A., et al. 1989, Science, 246, 1422

Stevenson, D. J. 1993, in Lunar and Planetary Institute Conference Abstracts, 1355

Trafton, L. M., Hunten, D. M., Zahnle, K. J., & McNutt, Jr., R. L. in Pluto and Charon, ed. S.A. Stern, D.J. Tholen (Tuscon: University of Arizona Press) 475

Trujillo, C. A., Brown, M. E., Barkume, K. M., Schaller, E. L., & Rabinowitz, D. L. 2007, Astrophysical Journal, in press

Trujillo, C. A., Brown, M. E., Rabinowitz, D. L., & Geballe, T. R. 2005, Astrophysical Journal, 627, 1057

Young, E. F. & Binzel, R. P. 1993, Icarus, 102, 134

Chapter 6

Detection of Methane on Kuiper Belt Object (50000) Quaoar

This chapter has been published in its entirety under the same title by authors E.L. Schaller and M.E. Brown in *Astrophysical Journal Letters* 2007, Volume 670, p. 49–51.

6.1 Abstract

The near-infrared spectrum of (50000) Quaoar obtained at the Keck Observatory shows distinct absorption features of crystalline water ice, solid methane and ethane, and possibly other higher order hydrocarbons. Quaoar is only the fifth Kuiper belt object on which volatile ices have been detected. The small amount of methane on an otherwise water ice dominated surface suggests that Quaoar is a transition object between the dominant volatile-poor small Kuiper belt objects (KBOs) and the few volatile-rich large KBOs such as Pluto and Eris.

6.2 Introduction

While once Pluto and Triton were the only objects in the outer solar system known to contain volatile ices on their surfaces, the recent discoveries of frozen methane on the large Kuiper belt objects (KBOs) Eris, Sedna, and 2005 FY9 have shown that these objects are part of a new class of surface volatile rich bodies in the outer solar system (Brown et al., 2005; Licandro et al., 2006; Barucci et al., 2005; Brown et al., 2007). In contrast to these bodies with detectable volatiles, spectral observations of small KBOs over the past decade have found that most of these objects either contain varying amounts of involatile water ice on their surfaces or have flat spectra with no identifiable features (Barkume et al., 2007). To understand the dichotomy between volatile rich and volatile free surfaces in the outer solar system, Schaller & Brown (2007) constructed a simple model of atmospheric escape of volatile ices over the age of the solar system. They found that while most KBOs are too small and hot to retain their initial volatile ices to the present day, a small number are large and cold enough to retain these ices on their surfaces.

As anticipated, the model suggests that the largest KBOs, Eris, Pluto, and Sedna are all expected to retain surface volatiles, while the vast majority of the other known objects in the Kuiper belt are expected to have lost all surface volatiles. Two known

intermediate-sized KBOs are predicted to be in the transition region where they may have differentially lost some volatile ices (N_2) but retained others (CH_4). One of these transition objects, 2005 FY9, with a diameter of ∼1450 km (Stansberry et al., 2007) does indeed appear to contain abundant CH_4 but be depleted in N_2.

The other object that appears to be in the volatile non-volatile transition region is Quaoar, with a diameter of 1260±190 km(Brown & Trujillo, 2004). The infrared spectrum of Quaoar does not resemble that of 2005 FY9, however. Quaoar's spectrum is dominated by absorptions due to involatile water ice, which is not detected at all on 2005 FY9. In addition, Jewitt & Luu (2004) reported the detection of an absorption feature near 2.2 μm that they attributed to ammonia hydrate. They also detected the presence of crystalline water ice which, at the $\sim$ 40 K radiative equilibrium temperature of Quaoar, is thought to be converted to amorphous water ice on a relatively short ($\sim$ 10 Myr) timescale by cosmic ray bombardment. The crystallinity of the water ice and the detection of the 2.2 μm feature that they attributed to ammonia hydrate led Jewitt & Luu (2004) to suggest that Quaoar may have experienced relatively recent cryovolcanic activity.

In this paper, we present a new infrared spectrum of Quaoar with a signal-to-noise in the K-band six times greater than that of Jewitt & Luu (2004) and model the ices present on the surface.

6.3 Observations

Near-infrared spectra of Quaoar were obtained on 12 July 2002, and 23, 24 and 25 April 2007 using NIRSPEC, the facility medium to high resolution spectrometer on the Keck telescope (McLean et al., 1998). Three separate grating settings were used to completely cover the region from 1.4 to 2.4 μm. The 1.44-1.73 and 1.70-2.13 μm regions were each covered in 6 exposures of 200 seconds each and the 2.0 to 2.4 μm region was covered in 82 exposures of 300 seconds each. Observations consisted of a

series of exposures on two or three nod positions along the 0.57" slit. All observations were performed at an airmass of better than 1.5. Data reduction was carried out as described in Brown (2000). Telluric calibration was achieved by dividing the spectra by nearby G dwarf stars observed at an airmass within 0.1 of that of the target.

Figure 1 shows the complete near-infrared spectrum of Quaoar. The absolute value of the infrared albedo is obtained from the R albedo of $0.092^{+0.036}_{-0.023}$ (Brown & Trujillo, 2004) , the V-R color of 0.64 ± 0.04, and an estimated V-J color of 2.1 ± 0.2 using typical values found by McBride et al. (2003). Errors in the overall absolute albedo calibration are of the order of 30% and are dominated by the uncertainty in the optical albedo.

The characteristic broad absorptions due to water ice are apparent at 1.5 and 2.0 μm. In addition, the presence of the unique crystalline water ice feature at 1.65 μm indicates that at least some of the water ice is in crystalline form. We also detect the absorption feature at 2.2 μm previously attributed to ammonia hydrate as well as a series of broad absorption features beyond 2.25 μm.

6.4 Spectral Modeling

We first attempt to model the spectrum of Quaoar with a mixture of water ice and a dark featureless material. Using the bidirectional reflectance models of Hapke (1993) we model a spatially segregated mixture of crystalline water ice grains (Grundy & Schmitt, 1998) and a dark red material. Optical path length was parameterized as a grain size in a scattering regolith. In order to investigate the additional absorption features longward of 2.1 μm not due to water ice, we performed a least-squares best fit to the 1.4 to 2.1 μm region where the fractional abundance of the ice, the grain size of the ice, and the color of the dark material were allowed to vary. Figure 1a shows the best-fit model with 10 μm water ice grain sizes, an ice fraction of 40% linearly mixed with a red continuum with a spectral slope of 10% per μm and an albedo of

13% at 2 μm. The spectrum could be equally well fit with a model where water ice was significantly more abundant and the dark material was intimately mixed, rather than linearly mixed, with the ice.

The water ice model provides a good fit to the data from 1.4 to 2.1 μm, and, as expected, deviates in the region beyond 2.1 μm. In order to explore the spectral shape of the deviation beyond 2.1 μm, we show, in Figure 2a, the ratio of the Quaoar spectrum to the water ice model. In addition to the 2.2 μm feature seen by Jewitt & Luu (2004), we see additional distinct but broader absorption features at 2.32 and 2.38 μm. The locations and depths of these three absorption features as well as the general shape of the ratio spectrum beyond 2.1 μm are well fit by absorptions due to methane ice. A model methane spectrum using the laboratory data of Grundy et al. (2002) with 100 μm grain sizes provides an excellent fit to the 2.0 - 2.4 μm ratio spectrum. In addition, smaller absorptions at 1.8 and 1.72 μm are also well fit by methane (Figure 1b). We measured the band center of the 2.2 μm feature to be at 2.205$\pm$0.002 which is consistent with that expected from pure methane (Quirico & Schmitt, 1997). Hydrated ammonia, in contrast, has a single absorption in this region at a wavelength between 2.21 and 2.24 μm, depending on the degree of hydration (Moore et al., 2007). While the Quaoar absorption feature at 2.205$\pm$0.002 is perhaps consistent with the 2.21 μm wavelength of the absorption feature of the most hydrated ammonia, ammonia cannot explain any of the additional major absorptions seen on Quaoar, all of which are well explained by the presence of methane. We thus conclude that the absorption feature initially attributed to ammonia is actually one of a series of absorption features caused by methane.

We can model the overall spectrum of Quaoar with a linear mixture of 35% water ice, 5% methane, and 60% dark material. While most features of the spectrum are well fit by this model, additional absorptions near 2.27 μm still cannot be explained by methane (Figure 2b). On 2005 FY9, Brown et al. (2007) found that the surface contained not just volatile methane, but a small amount of involatile ethane, hy-

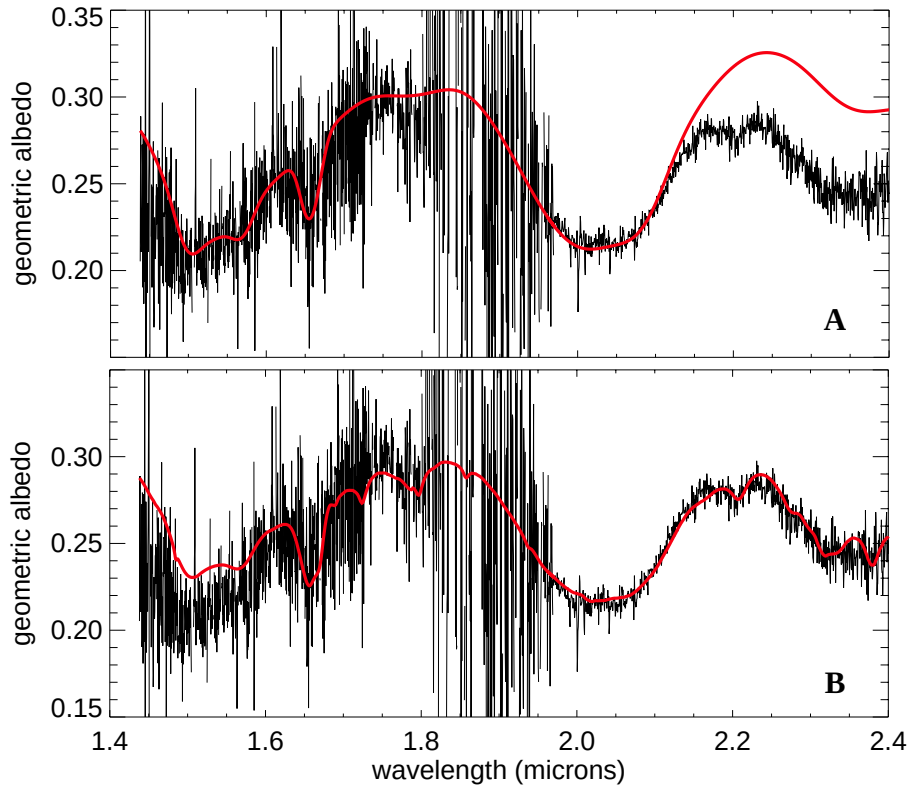

Figure 6.1 A. Near-infrared spectrum of Quaoar obtained with NIRSPEC on the Keck telescope (McLean et al., 1998). The signature of crystalline water ice is dominant. A best-fit water ice and dark red continuum model is shown. The major features of the spectrum are well fit by the model except for the 2.2-2.4 μm region where additional absorption occurs. B. Quaoar spectrum shown with the best-fit water ice, continuum, methane and ethane model. The presence of methane is required to fit the long wavelength end of the spectrum.

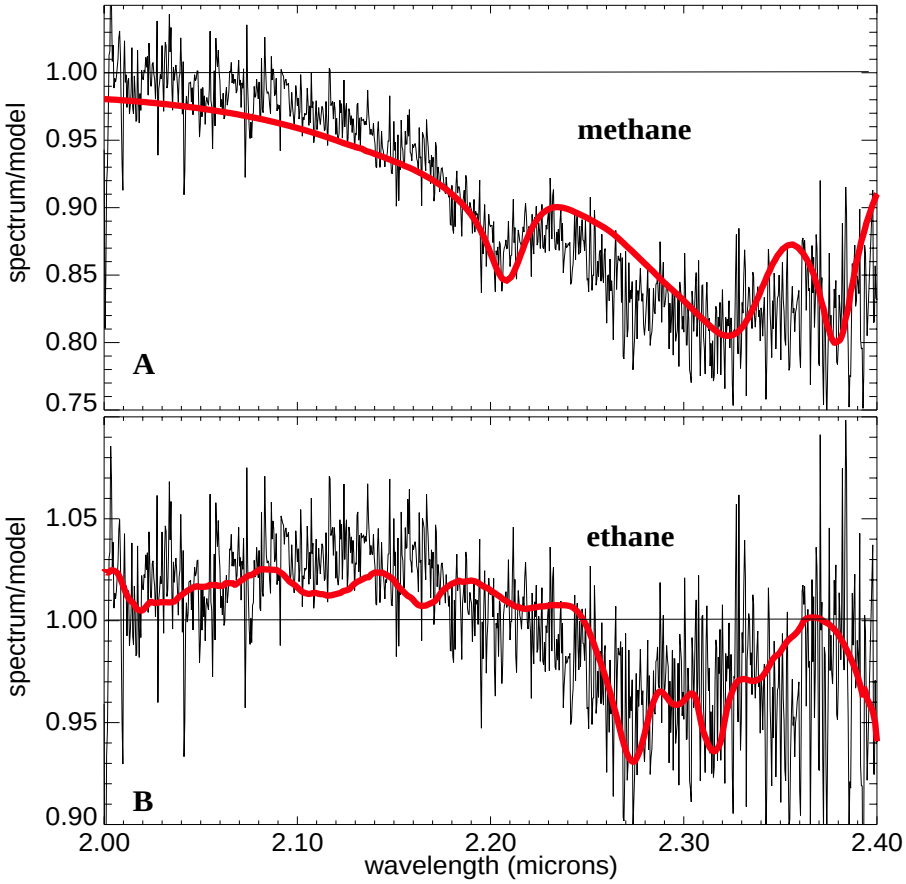

Figure 6.2 A. Ratio of the spectrum to the best-fit water ice and red continuum model. In addition to the 2.2 μm feature seen by Jewitt & Luu (2004), we see additional distict but broader absorption features at 2.32 and 2.38 μm which are well matched by methane. A model methane spectrum (Grundy et al., 2002) with 100 μm grain sizes provides an excellent fit to the ratio spectrum. B. Ratio of the spectrum to the best-fit water ice, continuum and methane model. While most features of the spectrum are well fit by this model, additional absorptions occur near 2.3 μm. The two strongest absorption features at 2.27 and 2.32 μm are well fit by ethane.

pothesized to derive from irradiation of the solid methane. The deviation from the methane spectrum on Quaoar also appears to be well fit, at least in part, by the presence of ethane. Figure 2b shows a model of 10 μm ethane grains constructed from the absorption coefficients of Quirico & Schmitt (1997). In particular, the two strongest absorption features at 2.27 and 2.32 μm are clearly detected as they are on 2005 FY9. An additional small absorption feature at 2.36 μm remains unidentified but may be due to a higher-order hydrocarbon.

Figure 1b shows the complete model fit with a spatial mixture of 35% water ice, 55% dark material, 6% methane and 4% ethane. While the specific values of these parameters have little unique meaning, as many different values could give similar fits, in general we find that methane and ethane are minority species on a water ice dominated surface. The slight increase in the albedo of our best-fit model in the 1.4-1.6 μm region compared to the spectrum indicates that a single sloped continuum in the infrared is insufficient. No evidence for other volatile species is detected; in particular, we did not detect the 2.148 μm N2 absorption feature nor the 2.352 μm CO absorption feature.

6.5 Discussion

With significantly higher signal-to-noise in the 2.0 - 2.4 μm region, the 2.2 μm absorption feature on Quaoar previously identified as ammonia hydrate (Jewitt & Luu, 2004) is clearly seen to be due to methane ice. No compelling evidence is seen for the presence of ammonia. The presence of crystalline water ice on the surface of Quaoar still remains unexplained because it is expected that ice should currently exist in the amorphous form on the $\sim$ 40 K surface of Quaoar. However, the presence of the 1.65 μm absorption feature due to crystalline water ice in the spectrum of every well observed water ice rich KBO (even down to diameters of only a few hundred kilometers) (Barkume et al., 2007) suggests that exotic processes such as cryovolcanism

are unlikely to be required. The presence of crystalline water ice on so many small outer solar system bodies may indicate that our current understanding of the physics of the crystalline/amorphous phase transition may not be complete. The spectrum of Quaoar is consistent with that of a cold geologically dead object slowly losing the last of its volatile ices by escape in a tenuous, perhaps patchy, atmosphere.

Ethane is an expected by-product of irradiation of methane ice (Baratta et al., 2003). The presence of ethane on Quaoar and on 2005 FY9 supports the suggestion of Brown et al. (2007) that these irradiation products are preferentially seen on bodies with large abundances of pure methane rather than on the bodies where the methane is diluted in nitrogen. Quaoar also appears to be rich in more complex irradiation products. Quaoar is the only water ice rich KBO which has a red color in the visible. Other water ice rich KBOs like Orcus, Charon, and 2003 EL61 and its family of collisional fragments are all blue in the visible (Barkume et al., 2007). Quaoar's red surface is likely due to the continued irradiation of methane, ethane, and their products on the surface (Brunetto et al., 2006).

While methane on Quaoar is sufficiently volatile that it is likely to seasonally migrate if Quaoar has a moderate obliquity, ethane and the other irradiation products are essentially involatile at Quaoar's temperature. Quaoar is therefore likely to have an irregular covering of irradiation products, perhaps leading to rotational variability in its visible color and in the abundance of ethane. Continued observations of this object will provide insight into the nature of the volatile non-volatile transition and atmospheric escape in the outer solar system.

Acknowledgments: We thank an anonymous referee for a helpful review. E.L.S. is supported by a NASA Graduate Student Research Fellowship. The data presented herein were obtained at the W.M. Keck Observatory, which is operated as a scientific partnership among the California Institute of Technology, The University of California and the National Aeronautics and Space Administration. The observatory was made possible by the generous financial support of the W.M. Keck Foundation.

Bibliography

Baratta, G. A., Domingo, M., Ferini, G., Leto, G., Palumbo, M. E., Satorre, M. A., & Strazzulla, G. 2003, Nuclear Instruments and Methods in Physics Research B, 209, 283

Barkume, K. M., Brown, M. E., & Schaller, E. L. 2008, Astrophysical Journal, 135, 55

Barucci, M. A., Cruikshank, D. P., Dotto, E., Merlin, F., Poulet, F., Dalle Ore, C., Fornasier, S., & de Bergh, C. 2005, Astronomy and Astrophysics, 439, L1

Brown, M. E. 2000, Astronomical Journal, 119, 977

Brown, M. E., Barkume, K. M., Blake, G. A., Schaller, E. L., Rabinowitz, D. L., Roe, H. G., & Trujillo, C. A. 2007, Astronomical Journal, 133, 284

Brown, M. E. & Trujillo, C. A. 2004, Astronomical Journal, 127, 2413

Brown, M. E., Trujillo, C. A., & Rabinowitz, D. L. 2005, Astrophysical Journal, Letters, 635, L97

Brunetto, R., Barucci, M. A., Dotto, E., & Strazzulla, G. 2006, Astrophysical Journal, 644, 646

Grundy, W. M. & Schmitt, B. 1998, Journal of Geophysics Research, 103, 25809

Grundy, W. M., Schmitt, B., & Quirico, E. 2002, Icarus, 155, 486

Hapke, B. 1993, Theory of reflectance and emittance spectroscopy (Topics in Remote Sensing, Cambridge, UK: Cambridge University Press, —c1993)

Jewitt, D. C. & Luu, J. 2004, Nature, 432, 731

Licandro, J., Pinilla-Alonso, N., Pedani, M., Oliva, E., Tozzi, G. P., & Grundy, W. M. 2006, Astronomy and Astrophysics, 445, L35

McBride, N., Green, S. F., Davies, J. K., Tholen, D. J., Sheppard, S. S., Whiteley, R. J., & Hillier, J. K. 2003, Icarus, 161, 501

McLean, I. S., Becklin, E. E., Bendiksen, O., Brims, G., Canfield, J., Figer, D. F., Graham, J. R., Hare, J., Lacayanga, F., Larkin, J. E., Larson, S. B., Levenson, N., Magnone, N., Teplitz, H., & Wong, W. 1998, in Presented at the Society of Photo-Optical Instrumentation Engineers (SPIE) Conference, Vol. 3354, Proc. SPIE Vol. 3354, p. 566-578, Infrared Astronomical Instrumentation, Albert M. Fowler; Ed., ed. A. M. Fowler, 566–578

Moore, M. H., Ferrante, R. F., Hudson, R. L., & Stone, J. N. 2007, Icarus, 190, 260

Quirico, E. & Schmitt, B. 1997, Icarus, 127, 354

Schaller, E. L. & Brown, M. E. 2007, Astrophysical Journal, Letters, 659, L61

Stansberry, J., Grundy, W., Brown, M., Cruikshank, D., Spencer, J., Trilling, D., & Margot, J.-L. 2007, ArXiv Astrophysics e-prints